Research Square

Preprints are preliminary reports that have not undergone peer review.
They should not be considered conclusive, used to inform clinical practice,
or referenced by the media as validated information.

An adiponectin-frontothalamic pathway mediates the rapid antidepressant effects of acute exercise

Suk-Yu Yau

sonata.yau@polyu.edu.hk

The Hong Kong polytechnic university https://orcid.org/0000-0002-7425-6741

Douglas Formolo

Hong Kong Shue Yan University https://orcid.org/0000-0003-1908-8658

Tong Cheng

Jiasui Yu

Hui Zhang

Yunxiao Zhong

Zafar Iqbal

Natalia Formolo

Chun Hsu

Georg Kranz

The Hong Kong Polytechnic University https://orcid.org/0000-0002-3892-1804

Kangguang Lin

Kwok-Fai So

Jinan University https://orcid.org/0000-0003-4039-4246

Li Zhang

Jinan University https://orcid.org/0000-0003-1489-0879

Article

Keywords:

Posted Date: November 11th, 2026

DOI: https://doi.org/10.21203/rs.3.rs-11094381/v1

License: This work is licensed under a Creative Commons Attribution 4.0 International License.
Read Full License

Additional Declarations: There is **NO** Competing Interest.

FRONT MATTER

Title

An adiponectin-frontothalamic pathway mediates the rapid antidepressant effects of acute exercise

Authors

Douglas A. Formolo,[1,2*] Tong Cheng,[1*] Jiasui Yu,[1,3,4] Hui Zhang,[1] Yunxiao Zhong,[1,3,4] Zafar Iqbal,[1] Natalia P. S. Formolo,[1] Chun Liang Hsu,[1,3,4] Georg S. Kranz,[1,4] Kangguang Lin,[5] Kwok-fai So,[6] Li Zhang,[6] Suk-Yu Yau[1,3,4]#

Affiliations

[1]Department of Rehabilitation Sciences, Faculty of Health and Social Sciences, Hong Kong Polytechnic University, Hong Kong S.A.R., China.

[2] Department of Counselling and Psychology, Hong Kong Shue Yan University, Hong Kong S.A.R., China.

[3]Research Institute for Smart Ageing (RISA), Hong Kong Polytechnic University, Hong Kong S.A.R., China.

[4] Mental Health Research Center (MHRC), Hong Kong Polytechnic University, Hong Kong S.A.R., China.

[5] Department of Psychiatry, Faculty of Medicine, The Chinese University of Hong Kong (Shenzhen), Shenzhen, China

[6] Guangdong-Hong Kong-Macao Institute of CNS Regeneration Research, Jinan University, Guangdong, China

*Co-first author with equal contribution
#Corresponding author (sonata.yau@polyu.edu.hk)

Abstract

Conventional antidepressants suffer from a therapeutic lag, highlighting an urgent need for rapid-acting interventions vital to preventing clinical escalation and acute depressive crises. While acute exercise provides immediate antidepressant effects, the underlying body-brain mechanisms remain elusive. Here, we identify a frontothalamic circuit mediating the rapid behavioral benefits of acute running exercise. In rodents, glutamatergic projections from the anterior cingulate cortex (ACC) to the anterodorsal thalamus (AD) are necessary and sufficient to drive post-exercise behavioral rescue. This pathway is activated by the exercise-induced release of the systemic exerkine adiponectin, which acts via AdipoR1 in the ACC to recruit downstream AD projections. Translationally, adiponectin levels after a single session of acute exercise in humans correlate with increased frontothalamic functional connectivity. Our findings map an endocrine-frontothalamic axis governing rapid mood state transitions, offering a mechanistic blueprint for targeted "exercise prescriptions" to prevent acute depressive episodes.

Keywords:

MAIN TEXT

Introduction

Major depression is a leading global cause of disability (*1*, *2*), yet its therapeutic management is severely constrained by a critical clinical bottleneck. Traditional antidepressants suffer from a delayed onset of action of several weeks (*3*), while rapid-acting pharmacotherapies present significant safety, accessibility, and tolerability concerns (*4*, *5*). Consequently, there is an urgent need for safe, fast-acting interventions. Notably, engaging in acute exercise produces a rapid and dose-dependent alleviation of depressive symptoms in clinical populations (*6*) while buffering the physiological and emotional reactivity induced by repeated stress exposure (*7*, *8*). We have previously demonstrated that a single bout of exercise exerts rapid antidepressant-like effects in humans and rodents, with its action depending on activating glutamatergic neurons in the medial prefrontal cortex (mPFC) (*9*). However, its neural circuit mechanisms remain elusive. This critical knowledge gap not only hampers the clinical standardization of acute exercise-based therapies but also obscures fundamental physiological pathways that govern rapid mood regulation.

At the neurobiological level, a hallmark of rapid-acting pharmacological antidepressants is a glutamate-associated surge in PFC activity (*4*). This elevated activity is thought to increase global PFC functional connectivity (*10*, *11*) and enhance top-down regulation of downstream limbic structures (*12*), culminating in rapid mood elevation. Notably, we have recently demonstrated that the rapid antidepressant-like effects of a single bout of physical exercise rely on increased glutamatergic activity in the anterior cingulate cortex (ACC) of the mPFC (*9*). Similarly, clinical and preclinical studies have indicated that exercise-associated improvements in affect rely on enhanced

PFC-mediated top-down regulation of the limbic system (*13*, *14*). Yet, despite these striking parallels between rapid-acting pharmacological agents and physical exercise, the downstream projection targets of the PFC and the precise neural circuits that mediate the rapid antidepressant-like effects of exercise remain unknown.

Furthermore, adiponectin has been recognized as a key metabolic hormone that mediates exercise-associated crosstalk between adipose tissue and the brain (*9*, *15*, *16*). Adiponectin is an adipocyte-secreted hormone involved in metabolic regulation during energy depletion via activation of adiponectin receptors 1 (AdipoR1) and 2 (AdipoR2) (*17*, *18*). Given the tight energetic maintenance necessary for the appropriate functioning of the neural tissue (*16*, *19*), adiponectin deficiency has been implicated in several neurological and psychiatric disorders (*20*, *21*), including depression (*22*). On the other hand, increasing central adiponectin signaling reverses plasticity-associated neurological deficits (*23*) and leads to rapid antidepressant effects (*24*). Remarkably, we recently demonstrated that the rapid antidepressant effects of acute exercise are mediated by increased adiponectin-AdipoR1 signaling in the ACC (*9*).

Here, we sought to determine the specific ACC-associated downstream circuit mediating the rapid antidepressant effects of acute exercise and the role of adiponectin as a potential modulator of such circuit. By combining viral tracing, optogenetics, and chemogenetics in mice, we demonstrate that the rapid affective response to a single bout of running requires the activation of the ACC projections to the anterodorsal nucleus of the thalamus (AD), a process critically moderated by elevated adiponectin/AdipoR1 signaling within this circuit. Translated to a clinical cohort of healthy young adults, we further show that serum adiponectin levels immediately after a single running session positively correlate with increased functional connectivity between the ACC and the thalamus. Together, these translational findings reveal a

novel endocrine-neurocircuitry axis driving the immediate emotional benefits of physical exertion. By establishing this concrete mechanistic foundation, our work provides mechanistic insights supporting acute exercise as a potent, validated rapid remedy for alleviating depressive mood**,** transforming a general wellness recommendation into a precise, fast-acting non-pharmacological clinical intervention.

Results

Activation of glutamatergic neurons in the ACC and AD is required for the rapid antidepressant-like effects of single-bout physical exercise

Our previous work demonstrated that acute exercise modulates c-Fos expression across 17 brain regions (*9*). To map the network-level organization of this response, we performed a graph-theoretic analysis of these data, defining functional connections as positive correlation in pairwise c-Fos expression levels between two brain regions (*25*, *26*). The network analysis revealed that in exercised mice, the ACC and the AD serve as central hubs, exhibiting the highest degree of functional connectivity (Fig. 1a-f). Such hub-like properties implicate the ACC and AD as critical coordinators of the immediate central effects of acute exercise.

Using a separate cohort of mice, we characterized the cell-type-specific identity of the activated neurons in the ACC and AD (Fig. 2a). Acute exercise significantly increased c-Fos expression in the ACC (Fig. 2b), with the majority of c-Fos$^+$ cells co-expressing the glutamatergic marker Ca2+/calmodulin-dependent protein kinase II (CaMKII) rather than GABA (Fig. 2c-d). In the AD, exercise increased c-Fos expression (Fig. 2e), which was predominantly localized to CaMKII-expressing neurons (Fig. 2f). Notably, consistent with previous publications (*27*), GABAergic cells were undetectable in the AD (Fig. 2g).

Together, these findings demonstrate that acute exercise preferentially recruits glutamatergic neurons in both the ACC and AD.

To determine whether the activation of glutamatergic neurons in the ACC or AD is necessary for the antidepressant effects of acute exercise, we employed a chemogenetic approach. CaMKII-Cre transgenic mice received bilateral microinjection of a Cre-dependent inhibitory DREAD reporter (AAV-DIO-hM4Di-mCherry) into either the ACC or AD to selectively silence glutamatergic neurons before acute exercise (Fig. 3a). Three weeks post-surgery, mice were administered clozapine-N-oxide (CNO, 1 mg/kg, i.p.) 30 minutes prior to a single session of treadmill running, followed by behavioral tests. Chemogenetic inhibition of glutamatergic neurons in either the ACC (Fig. 3b-d) or the AD (Fig. 3e-g) completely abolished the exercise-induced increase in grooming time in the sucrose splash test (SST) 2 hours post-exercise (Fig. 3c and 3f). Furthermore, this manipulation prevented the exercise-induced reduction in immobility time during the tail suspension test (TST) 24 hours post-exercise (Fig. 3d and 3g). These findings demonstrate that glutamatergic activity in the ACC and AD is indispensable for the rapid antidepressant-like effects of acute exercise.

The ACC sends glutamatergic projections to the AD

Although the topological mapping of thalamocortical projections indicates that the ACC sends ipsilateral and unidirectional projections to the AD (*28*), the neurochemical identity of this pathway remains unknown. To characterize this projection, we microinjected the retrograde fluorescent tracer cholera toxin B subunit (CTB) in the AD and performed immunohistochemistry to identify the neuronal types in the ACC projecting neurons (Fig. 4a). We observed CTB^{+} cells retrogradely labeled soma throughout the mPFC, with the highest density of projection neurons located in the ACC, followed by the prelimbic

(PL) cortex (Fig. 4b). Notably, the vast majority of CTB+ projection neurons in the ACC co-localized with CaMKII (~96%; Fig. 4c) rather than GABA (Fig. 4d–e), indicating that the ACC–AD pathway is predominantly glutamatergic. To validate this monosynaptic connectivity, we utilized an anterograde tracing strategy by injecting an AAV1-Cre vector into the ACC and a Cre-dependent reporter (AAV-DIO-EGFP) into the AD (Fig. 4f and Fig. S1a). Three weeks post-injection, EGFP+ve cells were detected in the AD (Fig. 4g) and selectively co-localized with CaMKII (Fig. 4h) but not with GABA markers (Fig. S1b). Together, these retrograde and anterograde tracing results establish the glutamatergic nature of the ACC–AD circuit.

The ACC-AD pathway mediates the rapid antidepressant-like effects of single-bout physical exercise

To establish the functional necessity of the ACC-AD pathway in mediating the rapid effects of acute exercise, we employed chemogenetic modulation of the ACC-AD circuit. Wild-type mice were injected with a retrograde Cre recombinase vector (AAVrg-Cre) in the AD and a Cre-dependent inhibitory DREAD (AAV-DIO-hM4Di-mCherry) in the ACC. All animals were treated with CNO to selectively silence ACC neurons projecting to the AD (Fig. 5a-b). Administering CNO 30 minutes prior to acute exercise did not change baseline behavior in sedentary control mice (Fig. 5c-d). Conversely, inhibiting the ACC-AD circuit completely blocked the exercise-induced antidepressant-like effects in both the SST (Fig. 5c) and TST (Fig. 5d), demonstrating that the ACC–AD circuit is indispensable for the rapid antidepressant-like effects of acute exercise. Crucially, in a separate cohort, circuit silencing did not alter total distance traveled or time spent in the center of the open field test (OFT) (Fig. S2a-c), confirming that these behavioral effects were not confounded by deficits in general locomotor activity or altered anxiety-like/avoidance behavior.

To determine whether activating this pathway is sufficient to recapitulate the antidepressant-like effects of acute exercise in sedentary mice, we injected wild-type mice with the AVVrg-Cre in the AD and the AAV-DIO-hM3Dq-mCherry in the ACC (Fig. 5e). Sedentary mice were treated with CNO and subjected to behavioral testing. Chemogenetic activation of the ACC–AD circuit increased grooming time in the SST at 2 hours post-injection (Fig. 5f) and decreased immobility in the TST at 24 hours post-injection (Fig. 5g), effectively mimicking the acute exercise-induced behavioral performance. This manipulation did not alter anxiety-like behavior (Fig. 5h) or spontaneous locomotor activity in the OPF (Fig. 5i). Functional activation of the projection was histologically confirmed by a nearly 40-fold increase in downstream AD c-Fos expression (Fig. 5j). Collectively, these loss- and gain-of-function findings demonstrate that the ACC–AD circuit is both necessary and sufficient to drive the rapid antidepressant-like effects of acute exercise. To resolve the precise temporal necessity of this circuit and avoid the prolonged effects of chemogenetics (*29*), we further used optogenetics to inhibit the pathway specifically during exercise. We expressed AAV-DIO-eNpHR3.0-EGFP in the ACC of CaMKII-Cre mice and targeted their projection terminals in the AD with bilateral optic fibers (Fig. 6a-b). Restricting optogenetic inhibition to the active running period fully blocked the rapid antidepressant-like effects of exercise in both the SST (Fig. 6c) and the TST (Fig. 6d).

Next, to determine whether direct, brief pathway stimulation could serve as an efficient surrogate for physical exertion to rapidly alleviate depressive states, we tested whether optogenetic activation of this circuit in sedentary mice could replicate the benefits of running. We delivered a Cre-dependent channelrhodopsin vector (AAV-DIO-hChR2-EGFP*P*) into the ACC and targeted the AD terminals with light stimulation for 30 minutes, matching the duration of the active exercise protocol (Fig. 6e-f). Remarkably,

this brief, targeted stimulation in sedentary animals was sufficient to increase grooming in the SST (Fig. 6g) and reduce immobility time in the TST (Fig. 6h), resembling the rapid behavioral improvement triggered by acute exercise. Successful circuit recruitment was histologically confirmed by robust downstream c-Fos expression in the AD (Fig. 6i). Together, these findings demonstrate that the ACC–AD pathway is a key circuit substrate that directly mediates the rapid therapeutic benefits of acute exercise.

Adiponectin mediates acute exercise-induced activation of the ACC-AD circuit

Our previous work established adiponectin as a key metabolic hormone required for the antidepressant effects of acute and chronic exercise (*9*, *15*, *16*). Building on these insights, we investigated whether central adiponectin signaling drives the activation of the ACC–AD circuit. We first assessed how a single bout of exercise modulates systemic and central adiponectin levels in wild-type mice, and evaluated whether exercise-induced neuronal activation is blunted in adiponectin-deficient (Adipo$^{-/-}$) mice (Fig. 7a). In wild-type mice, while serum adiponectin levels remained unaltered (Fig. 7b), adiponectin concentrations significantly rose in the ACC 30 minutes post-exercise (Fig. 7c), consistent with our prior report (*9*). Genetic deletion of adiponectin (Adipo$^{-/-}$) blunted the exercise-induced upregulation of c-Fos in both the ACC (Fig. 7d) and AD (Fig. 7e) without affecting baseline, sedentary expression levels.

To determine the behavioral consequences of this signaling deficit, we subjected a separate cohort of Adipo$^{-/-}$ and wild-type mice to post-exercise behavioral testing (Fig. 7f). Adiponectin deficiency fully ablated the therapeutic benefits of exercise, preventing both the increase in grooming time in the SST (Fig. 7g) and the reduction in immobility in the TST (Fig. 7h). Crucially, these behavioral deficits were not accompanied by alterations in general locomotion or anxiety-like behavior in the open field (Fig. S3a-b).

Together, these results demonstrate that central adiponectin is required for the rapid recruitment of the ACC–AD circuit and is an indispensable mediator of the acute antidepressant-like effects of exercise.

We next investigated whether acute elevation of central adiponectin signaling is sufficient to replicate the molecular and behavioral effects of physical exercise. Cannulated wild-type mice received a single intracerebroventricular (i.c.v.) microinjection of recombinant trimeric adiponectin (1 μg) two hours prior to perfusion (Fig. 8a). Immunohistochemical profiling revealed that central adiponectin administration significantly upregulated c-Fos expression in the ACC (Fig. 8b), This activation was highly selective for glutamatergic neurons, as shown by a high proportion of c-Fos+ cells co-localizing with CaMKII (Fig. 8c) rather than GABA (Fig. 8d). Similarly, central adiponectin increased c-Fos activation in downstream AD neurons (Fig. 8e), predominantly within the CaMKII-positive population (Fig. 8f). At the behavioral level, acute i.c.v. adiponectin infusion in a separate cohort recapitulated the rapid antidepressant-like effects of exercise, significantly increasing grooming in the SST and decreasing immobility in the TST (Fig. S4a-c), resembling the antidepressant-like effects of exercise. Moreover, it did not alter general locomotor activity or anxiety-like behavior in the open field (Fig. S4d-f).

Finally, we evaluated the functional requirement of the ACC–AD pathway in mediating these rapid neuroendocrine effects by chemogenetically silencing this circuit 30 minutes before central adiponectin administration (Fig. 8g-h). Intriguingly, chemogenetic inhibition of the ACC–AD pathway attenuated, but did not entirely abolish, the antidepressant-like actions of adiponectin. In circuit-inhibited mice treated with adiponectin, grooming times in the SST were still significantly elevated compared to vehicles, though to a lesser extent than in circuit-intact controls (Fig. 8i). Similarly,

the adiponectin-induced reduction in immobility was partially blunted but not fully blocked by circuit silencing (Fig. 8j). These results demonstrate that the ACC–AD pathway is a major, yet non-exclusive, neural substrate mediating the rapid antidepressant-like actions of central adiponectin.

Adiponectin–AdipoR1 signaling gates the acute exercise-induced activation of the ACC–AD pathway

Because elevated central adiponectin signaling mimics the effects of physical exertion, we next investigated whether local adiponectin-AdipoR1 signaling is required for the exercise-induced recruitment of the ACC–AD circuit. Having previously established that AdipoR1 is a critical molecular mediator of the rapid antidepressant benefits of exercise (*9*), we utilized an RNA interference strategy to selectively knock down AdipoR1 within ACC–AD projection neurons. We first validated the knockdown efficiency of a Cre-dependent AAV vector expressing an shRNA targeting AdipoR1 (AAV-DIO-shAdipoR1-RFP) in CaMKII-Cre mice (Fig. S5a-b). To restrict knockdown to the projection of interest, wild-type mice received AD microinjections of AAVrg-CreAAVrg-Cre and ACC microinjections of either control shRNA or AAV-DIO-shAdipoR1-RFP (Fig. 9a-b). Remarkably, projection-specific AdipoR1 knockdown blunted the exercise-induced increase in c-Fos expression in the ACC (Fig. 9c), This residual activation remained localized to glutamatergic populations, as the majority of c-Fos+ cells in both groups co-expressed CaMKII (Fig. 9d). A similar reduction in exercise-induced c-Fos expression was observed downstream in the AD (Fig. 9e), which was also predominantly restricted to CaMKII-expressing neurons (Fig. 9f). These findings demonstrate that AdipoR1 signaling within the ACC is necessary for the full functional recruitment of the ACC–AD projection during exercise.

To determine if this partial impairment in circuit activation translates to diminished behavioral efficacy, we knocked down AdipoR1 in the ACC–AD pathway in a separate behavioral cohort (Fig. 9g). Consistent with the immunohistochemical data, AdipoR1 knockdown attenuated, but did not completely abolish, the rapid antidepressant-like actions of exercise. Following a single running session, knockdown mice still exhibited a significant increase in grooming in the SST (Fig. 9h) and a decrease in immobility in the TST (Fig. 9i), though these improvements were significantly blunted compared to control animals. These behavioral differences were not confounded by alterations in anxiety-like behavior or spontaneous locomotor activity (Fig. S5c-d). Taken together, these results establish that the adiponectin–AdipoR1 axis is a key modulatory pathway required for the neurobiological and behavioral efficacy of acute exercise.

Increased post-exercise adiponectin levels correlate with frontothalamic functional connectivity in young adults

To translate our preclinical findings to humans, we investigated whether post-exercise peripheral adiponectin levels are associated with frontothalamic functional connectivity in young adults. We conducted a single-arm, pre-posttest clinical study wherein volunteers underwent resting-state functional magnetic resonance imaging (fMRI) and blood sampling before (pre-test) and after (post-test) a single 30-minute bout of moderate-intensity treadmill running (Fig. 10a). We reported that acute exercise significantly alleviated self-reported depressed mood (*9*). From an initial cohort of 40 participants (62.5% female, mean age 27.03 ± SD 5.25 years; Table S1), one participant was excluded from rest-state fMRI analysis due to data corruption (n=39), and 17 participants declined blood draws, yielding a final blood sample of n=23. Functional connectivity analysis (Fig. 10b) revealed that acute exercise did not globally alter

functional connectivity between the ACC and the left (Fig. 10c) or right thalamus (Fig. 10d). Furthermore, matching our observations in mice, circulating adiponectin levels did not significantly change immediately after exercise (Fig. 10e). Intriguingly, we observed a marginally significant, moderate positive correlation between post-exercise serum adiponectin levels and ACC–left thalamus functional connectivity (Fig. 10g, r_s = 0.40, p = 0.06), whereas no such relationship was found with the right thalamus (Fig. 10h). To assess the molecular specificity of this association, we measured brain-derived neurotrophic factor (BDNF), an activity-dependent neurotrophin known to increase with exercise (*30*) but shown not to mediate the acute mood-elevating effects of running (*31*). Although serum BDNF levels expectedly surged post-exercise (Fig. 10f), they showed no correlation with ACC-thalamic connectivity in either hemisphere (Fig. 10i-j). These data suggest that peripheral adiponectin may serve as a regulator of frontothalamic connectivity in humans following acute exercise.

Discussion

Although the neurobiological benefits of long-term exercise are relatively well-understood, the mechanisms driving the rapid mood-elevating responses to acute exercise have remained largely unknown. Here, we demonstrate that the acute antidepressant-like effects of a single exercise session rely on the functional recruitment of the ACC–AD glutamatergic projection, a process partially mediated by local adiponectin/AdipoR1 signaling within these ACC neurons. Using causal circuit manipulations in mice, we established that activating this frontothalamic projection is both necessary and sufficient to alleviate apathy and behavioral despair. Crucially, our human fMRI and biomarker data provide key translational validation, showing that post-exercise peripheral adiponectin levels selectively correlate with frontothalamic functional connectivity. By establishing a direct cross-species link between physical

exertion, neuroendocrine signaling, and circuit dynamics, these findings resolve a major bottleneck in clinical translation, offering a blueprint for rapid-acting, exercise-mimicking therapeutic strategies.

While previous studies have implicated the serotonergic system in mediating the affective benefits of exercise, our findings point to a distinct, cortical-glutamatergic mechanisms. In rats, a single bout of continuous treadmill running has been shown to increase neuronal activation in dorsal raphe nucleus (DRN) serotonergic neurons, correlating with reduced anxiety and behavioral despair (*31*, *32).* However, attributing acute anxiolytic effects to increased DRN serotonergic activation is difficult to reconcile with established literature; indeed, direct acute activation of DRN serotonergic neurons has been shown to promote, rather than reduce, anxiety-like behaviors (*32*). Therefore, exercise-associated serotonergic signaling may not fully account for these rapid behavioral improvements (*33*, *34*)

By dissecting a corticothalamic network, we demonstrated that the activation of glutamatergic projections from the ACC to the AD is both necessary and sufficient to drive the rapid antidepressant-like effects of acute exercise. The AD is a subregion of the anterior nuclei of the thalamus (ANT), a structure whose role in depression was previously unmapped but is increasingly recognized as vital to mood regulation. For example, downregulating ANT excitability via deep brain stimulation for drug-resistant epilepsy can trigger lasting psychiatric side effects (*35*). Furthermore, postmortem analyses reveal altered neuronal density specifically in the ANT of depressed patients compared to healthy controls (*36*). Clinically, patients with stroke lesions localized to the ANT experience significantly higher rates of depression and anxiety than those with lesions in other thalamic regions—onset occurs as early as one month post-stroke and persists for up to two years (*37*). Remarkably, targeting the ANT with transcranial

ultrasound stimulation has been shown to improve subjective depression scores within hours of treatment (*38*). Our results build on these clinical observations by identifying the AD as the critical cellular node within the ANT that gates rapid antidepressant responses, highlighting its promise as a target for non-invasive neuromodulation.

To identify the upstream trigger of this ACC-AD circuit during exercise, we focused on the adiponectin/AdipoR1 signaling pathway. Adiponectin receptors are expressed throughout the brain (*39–41*), with the AdipoR1 subtype exhibiting higher neuronal expression than AdipoR2 (*42*) and playing a documented role in mood regulation. For instance, knocking down AdipoR1 (but not AdipoR2) in neural progenitor cells blocks the proliferative, neurogenic effects of sustained exercise (*15*). Similarly, selectively knocking out AdipoR1 in DRN serotonergic neurons (*43*) or ventral tegmental area (VTA) dopaminergic neurons (*44*) induces depressive phenotypes, increases stress susceptibility, and abolishes the antidepressant effects of local adiponectin administration. Our study expands this literature by showing that acute physical exercise recruits peripheral-central signaling via adiponectin/AdipoR1 to activate the ACC-AD projection, establishing a direct link between physical exertion and rapid cortical circuit remodeling.

Translating these rodent circuit insights to humans, we recruited healthy young adults to participate in a single-arm pre-posttest study examining the effects of exercise on adiponectin levels and frontothalamic connectivity. In this cohort, we did not observe a significant increase in circulating adiponectin levels immediately after acute exercise, a finding that parallels our observations in mice and aligns with previous reports in healthy, untrained individuals (*45*). The absence of a systemic increase, however, does not negate the central role of adiponectin signaling in mediating the rapid mood-elevating effects of exercise. Several factors may account for this apparent discrepancy.

First, unlike other exercise-responsive adipokines, adiponectin circulates at relatively high basal concentrations (in the milligram-per-milliliter range) (*46*), which may render acute, transient changes difficult to detect in peripheral blood, particularly when sampling is limited to the immediate post-exercise time point. Second, emerging evidence suggests that exercise-induced adiponectin signaling may be compartmentalized (*47*), with functionally relevant changes occurring locally within specific brain regions rather than being uniformly reflected in the systemic circulation. Indeed, our prior work demonstrated that acute exercise increases adiponectin levels specifically within the medial prefrontal cortex of mice, without corresponding changes in serum (*9*). Notably, studies in trained individuals performing high-intensity exercise have reported detectable increases in post-exercise serum adiponectin (*48*, *49*), suggesting that exercise intensity and training status may critically influence the peripheral adiponectin response. Despite the lack of pre-posttest changes in our human cohort, we observed a significant positive correlation between post-exercise serum adiponectin levels and frontothalamic functional connectivity, specific to adiponectin rather than BDNF. By demonstrating this correlation, our clinical data support the hypothesis that the adiponectin–frontothalamic axis is actively engaged during acute physical exercise, validating the translational relevance of our rodent circuit model. Future studies incorporating additional post-exercise time points and more sensitive detection methods will be necessary to fully characterize the temporal dynamics of peripheral adiponectin and its relationship to the rapid antidepressant response in humans.

Given the challenges associated with managing depression symptoms, particularly during the lag phase of traditional therapies, dissecting the specific mechanisms mediating the rapid antidepressant-like response of acute physical exercise is a highly

timely endeavor. Our results unveil the ACC-AD glutamatergic pathway as a critical substrate for these rapid behavioral benefits and implicate the exercise-induced adiponectin/AdipoR1 cascade as a vital bridge across the body-brain axis. Beyond exercise, this circuit may also represent a common pathway shared by other rapid-acting psychiatric interventions. For example, altered thalamic gating of sensory and emotional stimuli via 5-HT2A receptor activation is hypothesized to drive the rapid effects of serotonergic psychedelics (*50*), reinforcing the idea that cortical-thalamic circuits are central to rapid depression relief.

Nonetheless, several limitations must be acknowledged when translating these findings to clinical practice. First, our clinical cohort was relatively small and consisted primarily of healthy individuals, meaning further research is required to determine if these acute benefits extend to patients with severe and/or treatment-resistant depression. Second, our human study relied on peripheral serum measures of adiponectin and did not provide direct evidence of localized activation of the ACC-AD circuit in the human brain. Future translational studies using advanced neuroimaging techniques, such as magnetic resonance spectroscopy (MRS), will be critical for confirming whether peripheral adiponectin fluctuations directly modulate ACC-thalamic connectivity in depressed patients. Third, our rodent experiments were carried out solely in males, which limits the generalizability of our circuit-level findings to females. Whether the ACC–AD glutamatergic pathway and its adiponectin-dependent regulation are similarly engaged in female mice following acute exercise remains an open question. This is particularly relevant given well-documented sex differences in the prevalence and clinical presentation of depressive disorders (*51*). Future investigations should directly compare male and female animals to determine whether the adiponectin–ACC–AD axis

operates equivalently across sexes, or whether alternative or compensatory mechanisms are recruited in females.

Ultimately, by providing detailed mechanistic insights into the rapid antidepressant effects of acute physical exercise, our characterization of a novel adiponectin-frontothalamic axis provides scientific evidence for these effects. The findings also pave the way for rapidly recalibrating thalamocortical gating, offering rapid relief of depressive mood, bypassing the therapeutic lag of traditional pharmacological antidepressants, and providing immediate, accessible relief from debilitating affective symptoms.

Materials and Methods

Animal experimental design

Male C57BL/6J mice (6-10 weeks old) were provided by the Centralized Animal Facility (CAF) of the Hong Kong Polytechnic University (PolyU). Animals were group-housed and maintained in a temperature-controlled holding room (22 ± 2 °C) under a 12-hour light-dark cycle (lights on at 8:00 AM), with *ad libitum* access to food and water. Transgenic mice expressing Cre recombinase under the control of the calcium/calmodulin-dependent protein kinase II promoter (CaMKII-Cre) and adiponectin-knockout ($Adipo^{-/-}$) mice were bred on a C57BL/6J genetic background and housed under identical conditions. All experimental procedures were approved by the university's Animal Subjects Ethics Sub-Committee.

Acute exercise protocol

To investigate the neurobiological effects of physical exertion, mice underwent a single session of acute running on a motorized treadmill, as previously done (*9*). To prevent novelty-induced stress and procedural anxiety, mice were habituated to the treadmill apparatus for three consecutive days prior to the experimental session. Habituation consisted of 5 minutes of free exploration on the stationary treadmill lane on days 1 and 2 and a 5-minute warm-up stage on day 3. The acute exercise session was performed on day 4. Following a 5 m/min warm-up (5 minutes in total), the mice underwent 20 intervals of high-intensity running (30 m/min for 30 s), interspersed with low-intensity recovery periods (5 m/min for 60 s). The speed was escalated stepwise (15→20→25→30 m/min) at the start, and the exercise finished with a 5 m/min cool-down for 5 minutes. All training was performed on a treadmill set to a 25° incline. To avoid confounding stress-related endocrine responses, electric shocks were not employed; if a mouse drifted to the end of the lane and ceased running, it was gently prodded with a soft brush to encourage forward movement. Sedentary control mice remained undisturbed in their home cages throughout the exercise period.

Behavioral assessments

All behavioral assays were conducted in a dedicated testing suite maintained under constant ambient illumination and controlled temperature (22 ± 2°C). Mice were transported to the testing room at 11:00 AM and acclimated to the environment for at least 2 hours prior to testing. To minimize circadian confounds, all behavioral manipulations were performed between 1:00 PM and 5:00 PM. Experimental procedures and subsequent data analyses were conducted by an investigator blinded to the experimental groups. All behavioral trials were video-recorded and analyzed post hoc using automated tracking software or manual scoring by a blinded observer. All the behavioral testing procedures were the same as previously performed (*9*, *52–55*)

Open field test (OFT)

The OFT is used to evaluate spontaneous locomotor activity and avoidance behaviors (*56*). The testing apparatus consisted of a square acrylic arena (40×40×40 cm). Mice were individually placed in the arena facing one of the outer walls (with the starting corner randomized across subjects) and allowed to freely explore the enclosure for 5 minutes. Spontaneous locomotor activity was quantified as the total distance traveled (in meters) during the session. Anxiety-like avoidance behavior was indexed by the duration of time spent in the central zone, defined as the inner 20×20×20 cm square of the arena. All trials were recorded and analyzed using ANY-maze video tracking software (Stoelting Co., Wood Dale, IL, USA).

Sucrose splash test (SSP)

To assess motivation-like self-care behavior, we performed the sucrose splash test (SST) (*57*). This test quantifies stimulus-induced self-grooming, in which a reduction in grooming activity indicates apathy or depression-like behavior. Mice were placed individually in a clean, transparent cage. The dorsal coat of each mouse was sprayed with a 10% (w/v) sucrose solution to induce grooming. Following the spray, the behavior was recorded for 5 minutes, and the total duration of self-grooming (defined as licking, scratching, and washing of the face, head, or body) was manually scored by an investigator blinded to the experimental groups.

Tail suspension test (TST)

To assess behavioral despair, mice were suspended by their tails (secured with adhesive tape approximately 1.5 cm from the tip) 50 cm above the floor for 6 minutes. A lightweight plastic cylinder was placed around the base of the tail to prevent tail-

climbing. Sessions were video-recorded and analyzed by an observer blinded to experimental groups. The duration of immobility for the last four minutes, defined as the complete absence of escape-directed movement, was manually quantified. The apparatus was cleaned with 70% ethanol between trials.

Stereotaxic surgery, microinjections, and cannula implantation

Mice were deeply anesthetized with a mixture of ketamine (100 mg/kg, i.p.) and xylazine (10 mg/kg, i.p.) and secured in a stereotaxic frame (RWD Life Science, Shenzhen, China). The scalp was disinfected with povidone-iodine, and a midline incision was made to expose the skull. The periosteum was removed using a dilute hydrogen peroxide solution to clearly visualize the bregma and lambda landmarks.

For intracerebroventricular (i.c.v.) cannulation, a unilateral craniotomy was performed over the right hemisphere, and a custom guide cannula (RWD Life Science) was lowered into the lateral ventricle (coordinates: AP −0.4 mm, ML −1.0 mm, DV −2.5 mm). The cannula was secured to the skull using three stainless steel anchor screws and dental cement (Lang Dental, Wheeling, IL, USA).

For tract-tracing and viral vector microinjections, small craniotomies were drilled over the ACC (unilateral for CTB, bilateral for AAVs; coordinates: AP +1.7 mm, ML ±0.4 mm, DV −1.8 mm) and the AD (bilateral; coordinates: AP −0.4 mm, ML ±0.8 mm, DV −3.5 mm). Microinjections of CTB or adeno-associated viruses AAVs were delivered into the ACC (0.2 μL per site) and AD (0.1 μL per site) at a constant rate of 0.1 μL/min using a 5-μL Hamilton syringe (Hamilton Co., Reno, NV, USA) driven by a microinfusion pump (11 Elite Nanomite, Harvard Apparatus, Holliston, MA, USA). Following infusion, the needle was left in place for an additional 5 minutes before gradual withdrawal to minimize fluid backflow.

For optogenetic experiments, bilateral ceramic optic fiber ferrules (200 μm core diameter, NA 0.37; RWD Life Science) were implanted targeting the AD. The coordinates were adjusted to position the fiber tips 100 μm dorsal to the injection site (DV −3.4 mm) and secured using anchor screws and dental cement.

Following surgery, the scalp incision was sutured, and mice received a subcutaneous injection of flunixin meglumine (2.5 mg/kg) for postoperative analgesia and anti-inflammatory support, which was maintained once daily for two consecutive days. Animals were allowed to recover for a minimum of 7 days before behavioral testing (for cannulation) or 3 weeks (to allow sufficient transgene expression for AAV-mediated manipulations).

Chemogenetics

To selectively modulate targeted neuronal populations and projection pathways, we used a chemogenetic approach utilizing the Cre-Lox system to drive the expression of double-floxed inverted open reading frame (DIO) Designer Receptors Exclusively Activated by Designer Drugs (DREADDs) (*29*, *58*). Cre recombinase was either expressed endogenously in glutamatergic excitatory neurons using transgenic CaMKII-Cre mice or introduced locally using viral vectors. AAV serotype 2 (AAV2) was selected for its high neuronal tropism, whereas AAV serotype 1 (AAV1) was utilized for its ability to undergo anterograde, trans-synaptic transport to target downstream postsynaptic neurons (*59*). For chemogenetic silencing, we used the human muscarinic G*i*-coupled receptor 4 (hM4Di; AAV2-hSyn-DIO-hM4Di-mCherry, titer: 5.3×10^{12}vg/mL, Addgene, Watertown, MA, USA). For chemogenetic activation, we used the human muscarinic *Gq*-coupled receptor 3 (hM3Dq; AAV2-hSyn-DIO-hM3Dq-mCherry, titer: 4.7×10^{12}vg/mL, Addgene). To achieve pathway-specific

(retrograde) targeting of projection neurons, a retrograde-transporting AAV encoding Cre recombinase (rAAV-pgk-Cre, titer: 1.0×10^{13} vg/mL, Addgene) was microinjected into the downstream projection terminal region, while DIO-DREADD vectors (or control vectors) were microinjected into the upstream somatic region. AAV2-hSyn-DIO-mCherry (titer: 3.2×10^{12} vg/mL, Addgene) was used as the fluorophore-only control across all cohorts.

Optogenetics

The Cre-Lox system was utilized to drive the expression of double-floxed AAV vectors in CaMKII-Cre mice (*60*, *61*). pAAV-EF1a-DIO-hChR2(H134R)-EGFP-WPRE-HGHpA (Addgene, USA) was used for excitation and pAAV-DIO-eNpHR-EGFP-WPRE-pA (Addgene, USA) for inhibition. AAVs were injected in the ACC while bilateral ferrules (RWD, China) were implanted above the AD to modulate the ACC glutamatergic terminals in AD. An AAV driving the expression of EGFP (AAV-pCAG-FLEX-EGFP-WPRE, Addgene, USA) was used as a control virus. Blue light (465 nm, 10 mW, 3 Hz, laser and waveform generator IOS-465/589, RWD, China) was delivered through a fiber optic cable (1.5 m) connected to the ferrules for photostimulation, while yellow light (589 nm) was used for photoinhibition. For photoinhibition during exercise, animals were habituated to the fiber optic cable (laser off) during the treadmill habituation protocol. On the experimental day, photoinhibition and exercise started simultaneously and lasted for the entire exercise. Sedentary animals remained in their home cages connected to the fiber optic cable with light delivered for forty minutes. For photoactivation, animals were similarly habituated to the fiber optic cable for three days. On the experimental day, mice were individually placed in a transfer cage and connected to the fiber-optic cable for photoactivation for forty minutes.

Retrograde and anterograde neuronal tracing

To map monosynaptic projection pathways between the ACC and the AD, we performed retrograde and anterograde tract-tracing experiments. For retrograde tracing, an Alexa Fluor 488-conjugated subunit B of cholera toxin (CTB-488; 1% w/v in PBS, Invitrogen, Carlsbad, CA, USA) was unilaterally microinjected into the AD (*27*). Seven days post-injection to allow for retrograde transport, brains were harvested, and CTB-labeled somas were quantified both ipsilaterally and contralaterally across the anteroposterior axis of the medial prefrontal cortex (mPFC; +2.10 to +1.54 mm relative to bregma) (*48*), specifically analyzing the ACC, prelimbic (PL), and infralimbic (IL) subregions. To confirm anatomical and functional connectivity from the ACC to the AD, we implemented a Cre-dependent, trans-synaptic anterograde tracing strategy. Mice received a bilateral microinjection of the anterogradely transported AAV1-Cre vector (pENN-AAV-hSyn-Cre-WPRE-hGH, Addgene) into the ACC, paired with bilateral microinjections of a Cre-dependent fluorophore vector (AAV-pCAG-FLEX-EGFP-WPRE, Addgene) into the downstream AD. This dual-vector approach restricted labeling only to those AD neurons receiving direct synaptic inputs from ACC projection terminals.

Pathway-specific knockdown of AdipoR1

To achieve pathway-specific knockdown of AdipoR1 in ACC neurons projecting to the AD (ACC-AD), we utilized a Cre-dependent short hairpin RNA (shRNA) silencing strategy. Mice received bilateral microinjections of a retrogradely transported AAV encoding Cre recombinase (rAAV-pgk-Cre, Addgene) into the AD to express Cre selectively in AD-projecting neurons. Concurrently, a Cre-dependent AAV driving the

584 expression of a double-floxed shRNA targeting AdipoR1 (AAV9-CMV-DIO-shRNA-
585 AdipoR1-RFP) was bilaterally microinjected into the upstream ACC.

586 A non-targeting scrambled sequence (AAV9-CMV-DIO-shRNA-Scramble-RFP) was
587 used as a control. Both the AdipoR1-targeting and scrambled control constructs were
588 synthesized and packaged by WZ Biosciences (Jinan, China). The shRNA target
589 sequence utilized to silence mouse AdipoR1 was: 5′-GCTTCGTTCCCTGGCTCTATT-
590 3′. Mice were allowed to recover for 3 weeks post-injection to ensure robust transgene
591 expression and target knockdown prior to behavioral and physiological evaluations.

592 *Drugs*

593 Recombinant trimeric adiponectin (ImmunoDiagnostics, Hong Kong) was reconstituted
594 in 0.01 M PBS to a stock concentration of 0.5 μg/μL and stored at −80°C. For i.c.v.
595 microinjections, a total dose of 1.0 μg (2.0 μL) of adiponectin was infused into freely
596 moving mice at a rate of 0.8 μL/min using a 5-μL Hamilton syringe connected to a
597 microinfusion pump (KD Scientific, Holliston, MA, USA). The internal injector cannula
598 was left in place for an additional 5 minutes post-infusion to prevent backflow. Clozapine
599 N-oxide (CNO; ApexBio, Houston, TX, USA) was dissolved in 0.15% dimethyl
600 sulfoxide (DMSO) in sterile physiological saline to a working concentration
601 of 0.1 mg/mL. CNO was freshly prepared on each experimental day and administered
602 intraperitoneally (i.p.) at a dose of 1.0 mg/kg approximately 30 minutes prior to
603 behavioral testing. Control groups received an equivalent volume of the saline/DMSO
604 vehicle.

605 *Immunohistochemistry*

Mice were deeply anesthetized and transcardially perfused with ice-cold phosphate-buffered saline (PBS), followed by 4% paraformaldehyde (PFA) in PBS. Brains were harvested, post-fixed overnight in 4% PFA at 4°C, and subsequently cryoprotected in a 30% (w/v) sucrose solution in PBS until they sank. Coronal sections (40 µm thick) were obtained using a vibratome (Leica Biosystems, Nussloch, Germany) and stored in a cryoprotectant solution at 4°C until processing. Free-floating immunofluorescence staining was performed to detect c-Fos (a nuclear marker of recent neuronal activation), *CaMKIIα* (a marker of glutamatergic excitatory neurons), and GABA (a marker of GABAergic inhibitory neurons). For cohorts not expressing fluorescent viral reporters, an antigen retrieval protocol was performed prior to antibody incubation: sections were incubated in a sodium citrate buffer (pH 6.0) at 95°C for 10 minutes, followed by treatment with 2 N hydrochloric acid (HCl) at 37°C for 10 minutes. For brain slices expressing AAV-derived fluorophores (mCherry or EGFP), this antigen retrieval step was omitted to preserve endogenous reporter fluorescence. Following three washes in PBS, sections were incubated overnight at room temperature with the following primary antibodies: mouse anti-c-Fos (1:250; Abcam, Cambridge, UK; RRID: AB_2631098), rabbit anti-CaMKIIα (1:200; Abcam; RRID: AB_301119), or rabbit anti-GABA (1:500; Sigma-Aldrich, St. Louis, MO, USA; RRID: AB_477652). The following day, sections were washed in PBS and incubated with corresponding fluorophore-conjugated secondary antibodies (1:200; Invitrogen, Carlsbad, CA, USA) for 2 hours at room temperature: goat anti-mouse Alexa Fluor 568, goat anti-mouse Alexa Fluor 488, goat anti-rabbit Alexa Fluor 568, or goat anti-rabbit Alexa Fluor 488. After final washes in PBS containing 4′,6-diamidino-2-phenylindole (DAPI; Sigma-Aldrich) for nuclear counterstaining, sections were mounted onto glass slides and coverslipped using an anti-fade fluorescence mounting medium (Dako, Carpinteria, CA, USA).

Confocal imaging and cell quantification

Z-stack confocal images (5–6 steps of 4 μm depth, 256×256×256 pixels) were acquired at 200× magnification using a Zeiss LSM 800 confocal microscope and ZEN software (Carl Zeiss, Jena, Germany). Maximum-intensity projection images were analyzed using FIJI (ImageJ, NIH, USA). Anatomical regions of interest (ROIs) were defined according to the mouse brain atlas across the following coordinates relative to bregma: mPFC subregions (ACC, PL, and IL; +1.94 to +1.54 mm) and AD (−0.34 to −0.94 mm) (*62*). For automated cell counting, a constant threshold was applied, and the "Analyze Particles" function was used to detect immunoreactive nuclei (size: 35–400 μm square; circularity: 0.3–1.0) (*63*). Cell density (particles/μm^2) was calculated for 2–3 sections per animal, averaged, and normalized to control levels. To determine neurochemical phenotypes, the percentage of c-Fos+, CTB+, or EGFP+ cells co-localizing with *CaMKIIα* or GABA was quantified within a randomized ACC ROI (≈70,000 μm square) or across the entire area of the AD.

Quantitative real-time polymerase chain reaction

To quantify *AdipoR1* transcript levels, prefrontal cortex (PFC) tissues were rapidly dissected from deeply anesthetized mice (isoflurane; Zoetis, Parsippany, NJ, USA). A 3-mm coronal slice containing the PFC was obtained using a brain matrix (RWD Life Science), bisected along the midline, snap-frozen in liquid nitrogen, and stored at −80°C. Total RNA was isolated using the ReliaPrep RNA Tissue Miniprep System (Promega, Madison, WI, USA) according to the manufacturer's instructions. Complementary DNA (cDNA) was synthesized from 2000 ng of total RNA using the GoScript Reverse Transcriptase kit (Promega) under the following conditions: annealing at 25°C for 5 minutes, extension at 42°C for 60 minutes, and heat

inactivation at 70°C for 15 minutes. Quantitative PCR was performed using the GoTaq qPCR Master Mix (Promega) with the following primer sequences: AdipoR1: forward 5'-GAAAGACAACGACTACCTGCTAC-3'; reverse 5'-CGTCAAGATTCCCAGAAAGAG3'; GAPDH: forward 5'-CCCATCACCATCTTCCAGGAGC-3'; reverse: 5'-CCAGTGAGCTTCCCGTTCAGC-3'. Target gene expression was normalized to *Gapdh* as the internal reference standard, and relative fold changes in gene expression were calculated using the comparative $2^{-\Delta\Delta CT}$ method.

Enzyme-linked immunosorbent assay (ELISA)

Serum was obtained by centrifuging cardiac blood samples collected from mice. Following the protocols established in our previous work (*9*), circulating adiponectin was quantified using a commercial ELISA kit (ImmunoDiagnostics Limited, Cat. No. 32010), with all serum samples diluted 600-fold prior to the assay. In parallel, proteins were extracted from dissected ACC tissues, and regional adiponectin levels were determined using a brain tissue-specific ELISA kit (AdipoGen Life Sciences, AG-45A-0004Y). To dissect the ACC, mice were perfused with normal saline, after which the brains were rapidly extracted. Each brain was placed ventral-side up on a Petri dish containing ice-cold PBS on ice, and the overlying meninges (arachnoid and pia mater) were peeled away with fine forceps. The intact brain was then positioned dorsal-side down in a chilled Mouse brain matrix (with 1 mm coronal slice intervals). An initial coronal cut was made at the olfactory bulbs (frontal pole) to create a flat anterior surface, followed by a secondary coronal cut between approximately Bregma +1.8 mm and +0.5 mm. Under a stereomicroscope, the ACC, which resides directly above the corpus callosum (comprising Areas 24a and 24b) and flanks the longitudinal fissure, was dissected from both hemispheres. The brain slice was held steady with forceps, and using a chilled

micro-punch tool, the ACC region was precisely extracted from the tissue directly above the corpus callosum, slightly lateral to the midline. The bilateral tissue samples were then pooled into small tubes and either used immediately for further analysis or preserved at -80°C until processing.

Clinical experimental design

A volunteer sample of 40 healthy adults (18 to 40 years old) was recruited for a single-arm, pre-posttest experiment (ClinicalTrials.gov, NCT06736067, Registration Date: May 12t^{h,} 2024), as previously described .(*9*) Participants had to be reportedly healthy and able to engage in moderate-intensity exercise. Participants were not considered for the study if they reported acute injury or illness, metabolic or neurological disorders, had iron implants, could not stand still, or were afraid of noise or enclosed spaces. Participants were recruited via an online form that included questions on basic sociodemographic information (sex and age) and the International Physical Activity Questionnaire (IPAQ) to assess physical activity levels. Eligible participants were invited to come to the University Research Facility in Behavioral and Systems Neuroscience (UBSN, PolyU) for the experimental session. On the day of the experimental session, participants were briefed about the experimental procedures and signed the informed consent form. Anthropometric measures were collected from participants, followed by the pre-test fMRI assessment. After the fMRI scan, participants completed mood-related questionnaires (reported in)(*9*), had a blood sample drawn via venipuncture, and began the exercise protocol. After the exercise session, participants rested for 5 minutes in a sitting position while posttest blood samples were drawn. Participants then completed the mood-related questionnaires once again, followed by the posttest scan. Twenty-three participants completed the entire experimental procedure, while 17 participants opted not

to withdraw blood before and/or after the exercise session. The project was approved by the Human Subject Ethics Sub-committee (HSEARS 20221111001).

fMRI image acquisition and analysis

Participants underwent MRI scanning on a Siemens 3 T Prisma scanner equipped with a 64-channel head coil. Structural images were acquired using a 3D T1-weighted TurboFLASH (TFL) sequence based on a magnetization-prepared rapid gradient-echo (MPRAGE) protocol. The parameters of this sequence included 320 sagittal slices, a repetition time (TR) of 2400 ms, an echo time (TE) of 2.13 ms, an inversion time (TI) of 1020 ms, a flip angle (FA) of 8 degrees, a field of view (FOV) of 224 × 224 mm^2, and a voxel size of 0.7 × 0.7 × 0.7 mm^3. Resting-state functional MR images (fMRI) were collected using a gradient-echo echo-planar imaging (GRE-EPI) sequence with the following parameters: TR = 800 ms, TE = 37 ms, FA = 52°, FOV = 218 × 250 × 144 mm^3, slice thickness = 2 mm, and 72 interleaved axial slices covering the whole brain. A total of 488 volumes were obtained, resulting in a scan duration of 6 min 39 s.

Resting-state fMRI data preprocessing and fractional amplitude of low-frequency fluctuation (fALFF) analysis were conducted using the Data Processing and Analysis for Brain Imaging (DPABI) toolbox in MATLAB R2023a. The preprocessing steps involved discarding the first ten time points to allow for magnetic field stabilization, followed by slice-timing correction to adjust for temporal differences among slice acquisitions and head-motion correction to realign functional volumes. The resting-state fMRI data were then coregistered to each participant's high-resolution 3D T1-weighted structural image, and the anatomical images were segmented into gray matter, white matter, and cerebrospinal fluid. In addition, the Diffeomorphic Anatomical Registration Through Exponentiated Liealgebra (DARTEL) tool (*64*) normalized the structural images and

tissue maps to Montreal Neurological Institute (MNI) space and created transformation parameters. Several nuisance variables, including white matter and cerebrospinal fluid signals and 24 head motion parameters, were regressed out. Both structural and functional images were spatially normalized to the Montreal Neurological Institute (MNI) space using deformation fields generated by the DARTEL algorithm during segmentation.

For fALFF computation, each voxel's time series was transformed into the frequency domain using a Fast Fourier Transform (FFT). The amplitude of low-frequency fluctuations (ALFF) was calculated as the square root of the averaged power within the 0.01–0.1 Hz frequency band. The fALFF was defined as the ratio of power within this band to the total power across the entire frequency spectrum. The resulting fALFF maps were then transformed using Fisher's z transformation (zfALFF) for subsequent statistical analyses. Region-of-interest (ROI) analysis was performed following zfALFF calculation. Frontal regions, including the ACC and thalamus, were defined based on the Automated Anatomical Labeling (AAL) template (*65*). All ROIs were extracted bilaterally. The mean zfALFF value within each ROI was then computed for every participant for further analysis.

Statistical analysis

Pairwise Pearson correlation tests exploring functional connectivity after exercise using the mice's whole-brain c-Fos data were performed using IBM SPSS Statistics 26.0 (IBM, USA). All remaining statistical analyses were performed using GraphPad Prism 10 (GraphPad Software, USA). Data distribution was analyzed using the Shapiro-Wilk test. Independent samples from two groups were analyzed by a two-tailed unpaired t-test or its non-parametric counterpart (Mann-Whitney test), while dependent samples were analyzed by paired-samples t-tests or the Wilcoxon Signed Rank Test. Multifactorial

analysis was performed by ANOVA, followed by the Tukey post-hoc test for multiple comparisons. Statistical significance was defined as a p-value < 0.05 (two-tail tests). Correlational analysis of functional connectivity and blood peripheral factors in human subjects were performed using Pearson's or Spearman's Rho test.

Data Availability

The datasets generated and/or analyzed during the current study are not publicly available due to institutional policies but are available from the corresponding author on reasonable request.

Code availability

No custom code was developed for this study. Analyses relied on standard, publicly available software packages (SPM and DPARSF for neuroimaging analyses; IBM SPSS Statistics and GraphPad Prism for statistical analyses); analysis parameters are described in the Methods.

References

1. T. Vos, S. S. Lim, C. Abbafati, K. M. Abbas, M. Abbasi, M. et al., Global burden of 369 diseases and injuries in 204 countries and territories, 1990–2019: a systematic analysis for the Global Burden of Disease Study 2019. *The Lancet* **396**, 1204–1222 (2020).
2. D. S. Hasin, A. L. Sarvet, J. L. Meyers, T. D. Saha, W. J. Ruan, M. Stohl, B. F. Grant, Epidemiology of Adult DSM-5 Major Depressive Disorder and Its Specifiers in the United States. *JAMA Psychiatry* **75**, 336–346 (2018).
3. A. A. Nierenberg, A. H. Farabaugh, J. E. Alpert, J. Gordon, J. J. Worthington, J. F. Rosenbaum, M. Fava, Timing of Onset of Antidepressant Response With Fluoxetine Treatment. *American Journal of Psychiatry* **157**, 1423–1428 (2000).
4. B. Kadriu, M. Greenwald, I. D. Henter, J. R. Gilbert, C. Kraus, L. T. Park, C. A. Zarate, Ketamine and Serotonergic Psychedelics: Common Mechanisms Underlying the Effects of Rapid-Acting Antidepressants. *Int. J. Neuropsychopharmacol.* **24**, 8–21 (2021).
5. G. S. Malhi, J. J. Mann, Depression. *The Lancet* **392**, 2299–2312 (2018).
6. J. Mata, R. J. Thompson, S. M. Jaeggi, M. Buschkuehl, J. Jonides, I. H. Gotlib, Walk on the bright side: Physical activity and affect in major depressive disorder. *J. Abnorm. Psychol.* **121**, 297–308 (2012).
7. J. Mata, C. L. Hogan, J. Joormann, C. E. Waugh, I. H. Gotlib, Acute exercise attenuates negative affect following repeated sad mood inductions in persons who have recovered from depression. *J. Abnorm. Psychol.* **122**, 45–50 (2013).

8. W. J. Rejeski, A. Thompson, P. H. Brubaker, H. S. Miller, Acute exercise: Buffering psychosocial stress responses in women. *Health Psychology* **11**, 355–362 (1992).
9. T. Cheng, D. A. Formolo, J. Yu, Y. Zhong, Z. Ma, A. Hussain, F. Natalia Paludo Silveira, L. Zhang, K. K. yip Cheng, G. S. Kranz, K. Lin, G. Chen, P. M. F. Siu, J. S. Yoo, C. S. W. Lai, A. Xu, K. F. So, S. Y. Yau, Rapid antidepressant effect of single-bout exercise is mediated by adiponectin-induced APPL1 nucleus translocation in anterior cingulate cortex. *Mol. Psychiatry* **30**, 5760–5776 (2025).
10. C. G. Abdallah, C. L. Averill, R. Salas, L. A. Averill, P. R. Baldwin, J. H. Krystal, S. J. Mathew, D. H. Mathalon, Prefrontal Connectivity and Glutamate Transmission: Relevance to Depression Pathophysiology and Ketamine Treatment. *Biol. Psychiatry Cogn. Neurosci. Neuroimaging* **2**, 566–574 (2017).
11. C. G. Abdallah, G. Sanacora, R. S. Duman, J. H. Krystal, The neurobiology of depression, ketamine and rapid-acting antidepressants: Is it glutamate inhibition or activation? *Pharmacol. Ther.* **190**, 148–158 (2018).
12. C. Li, M. Chen, W. Lin, C. Hong, B. Yang, R. Liu, P. Tu, T. Su, The effects of low-dose ketamine on the prefrontal cortex and amygdala in treatment-resistant depression: A randomized controlled study. *Hum. Brain Mapp.* **37**, 1080–1090 (2016).
13. L.-K. Ge, Z. Hu, W. Wang, P. M. Siu, G.-X. Wei, Aerobic Exercise Decreases Negative Affect by Modulating Orbitofrontal-Amygdala Connectivity in Adolescents. . **11**, 577 (2021).
14. T. S. Ligeza, I. Nowak, M. Maciejczyk, Z. Szygula, M. Wyczesany, Acute aerobic exercise enhances cortical connectivity between structures involved in shaping mood and improves self-reported mood: An EEG effective-connectivity study in young male adults. *International Journal of Psychophysiology* **162**, 22–33 (2021).
15. S. Y. Yau, A. Li, R. L. C. Hoo, Y. P. Ching, B. R. Christie, T. M. C. Lee, A. Xu, K.-F. So, Physical exercise-induced hippocampal neurogenesis and antidepressant effects are mediated by the adipocyte hormone adiponectin. *Proc. Natl. Acad. Sci. U. S. A.* **111**, 15810–5 (2014).
16. D. A. Formolo, T. Cheng, J. Yu, G. S. Kranz, S.-Y. Yau, Central Adiponectin Signaling – A Metabolic Regulator in Support of Brain Plasticity. *Brain Plasticity* **8**, 79–96 (2022).
17. T. Yamauchi, J. Kamon, Y. Minokoshi, Y. Ito, H. Waki, S. Uchida, S. Yamashita, M. Noda, S. Kita, K. Ueki, K. Eto, Y. Akanuma, P. Froguel, F. Foufelle, P. Ferre, D. Carling, S. Kimura, R. Nagai, B. B. Kahn, T. Kadowaki, Adiponectin stimulates glucose utilization and fatty-acid oxidation by activating AMP-activated protein kinase. *Nat. Med.* **8**, 1288–1295 (2002).
18. N. Kubota, W. Yano, T. Kubota, T. Yamauchi, S. Itoh, H. Kumagai, H. Kozono, I. Takamoto, S. Okamoto, T. Shiuchi, R. Suzuki, H. Satoh, A. Tsuchida, M. Moroi, K. Sugi, T. Noda, H. Ebinuma, Y. Ueta, T. Kondo, E. Araki, O. Ezaki, R. Nagai, K. Tobe, Y. Terauchi, K. Ueki, Y. Minokoshi, T. Kadowaki, Adiponectin Stimulates AMP-Activated Protein Kinase in the Hypothalamus and Increases Food Intake. *Cell Metab.* **6**, 55–68 (2007).
19. P. Mergenthaler, U. Lindauer, G. A. Dienel, A. Meisel, Sugar for the brain: the role of glucose in physiological and pathological brain function. *Trends Neurosci.* **36**, 587–597 (2013).
20. J. Bloemer, P. D. Pinky, W. D. Smith, D. Bhattacharya, A. Chauhan, M. Govindarajulu, H. Hong, M. Dhanasekaran, R. Judd, R. H. Amin, M. N. Reed, V. Suppiramaniam, Adiponectin Knockout Mice Display Cognitive and Synaptic Deficits. *Front. Endocrinol. (Lausanne).* **10**, 1–12 (2019).
21. R. C.-L. Ng, O.-Y. Cheng, M. Jian, J. S.-C. Kwan, P. W.-L. Ho, K. K.-Y. Cheng, P. K. K. Yeung, L. L. Zhou, R. L.-C. Hoo, S. K. Chung, A. Xu, K. S.-Ling. Lam, K. H. Chan, Chronic adiponectin deficiency leads to Alzheimer's disease-like cognitive impairments

and pathologies through AMPK inactivation and cerebral insulin resistance in aged mice. *Mol. Neurodegener.* **11**, 71 (2016).
22. R. Leo, G. Di Lorenzo, M. Tesauro, C. Cola, E. Fortuna, M. Zanasi, A. Troisi, A. Siracusano, R. Lauro, F. Romeo, Decreased plasma adiponectin concentration in major depression. *Neurosci. Lett.* **407**, 211–213 (2006).
23. R. C. Ng, M. Jian, O. K. Ma, M. Bunting, J. S. Kwan, G.-J. Zhou, K. Senthilkumar, A. Iyaswamy, P.-K. Chan, M. Li, K. M. Leung, S.-S. Kumar Durairajan, K. S. Lam, L. Chu, R. Festenstein, S. K. Chung, K. Chan, Chronic oral administration of adipoRon reverses cognitive impairments and ameliorates neuropathology in an Alzheimer's disease mouse model. *Mol. Psychiatry*, doi: 10.1038/s41380-020-0701-0 (2020).
24. J. Liu, M. Guo, D. Zhang, S.-Y. Cheng, M. Liu, J. Ding, P. E. Scherer, F. Liu, X.-Y. Lu, Adiponectin is critical in determining susceptibility to depressive behaviors and has antidepressant-like activity. *Proceedings of the National Academy of Sciences* **109**, 12248–12253 (2012).
25. G. Vetere, J. W. Kenney, L. M. Tran, F. Xia, P. E. Steadman, J. Parkinson, S. A. Josselyn, P. W. Frankland, Chemogenetic Interrogation of a Brain-wide Fear Memory Network in Mice. *Neuron* **94**, 363-374.e4 (2017).
26. A. L. Wheeler, C. M. Teixeira, A. H. Wang, X. Xiong, N. Kovacevic, J. P. Lerch, A. R. McIntosh, J. Parkinson, P. W. Frankland, Identification of a Functional Connectome for Long-Term Fear Memory in Mice. *PLoS Comput. Biol.* **9**, e1002853 (2013).
27. G. Vetere, F. Xia, A. I. Ramsaran, L. M. Tran, S. A. Josselyn, P. W. Frankland, An inhibitory hippocampal–thalamic pathway modulates remote memory retrieval. *Nat. Neurosci.* **24**, 685–693 (2021).
28. H. Shibata, J. Naito, Organization of anterior cingulate and frontal cortical projections to the anterior and laterodorsal thalamic nuclei in the rat. *Brain Res.* **1059**, 93–103 (2005).
29. G. M. Alexander, S. C. Rogan, A. I. Abbas, B. N. Armbruster, Y. Pei, J. A. Allen, R. J. Nonneman, J. Hartmann, S. SS. Moy, M. A. Nicolelis, J. O. McNamara, B. L. Roth, Remote Control of Neuronal Activity in Transgenic Mice Expressing Evolved G Protein-Coupled Receptors. *Neuron* **63**, 27–39 (2009).
30. R. E. Ross, M. E. Saladin, M. S. George, C. M. Gregory, High-Intensity Aerobic Exercise Acutely Increases Brain-derived Neurotrophic Factor. *Med. Sci. Sports Exerc.* **51**, 1698–1709 (2019).
31. J. D. Meyer, K. F. Koltyn, A. J. Stegner, J. S. Kim, D. B. Cook, Relationships between serum BDNF and the antidepressant effect of acute exercise in depressed women. *Psychoneuroendocrinology* **74**, 286–294 (2016).
32. D. J. Urban, H. Zhu, C. A. Marcinkiewcz, M. Michaelides, H. Oshibuchi, D. Rhea, D. K. Aryal, M. S. Farrell, E. Lowery-Gionta, R. H. J. Olsen, W. C. Wetsel, T. L. Kash, Y. L. Hurd, L. H. Tecott, B. L. Roth, Elucidation of The Behavioral Program and Neuronal Network Encoded by Dorsal Raphe Serotonergic Neurons. *Neuropsychopharmacology* **41**, 1404–1415 (2016).
33. T. Otsuka, A. Nishii, S. Amemiya, N. Kubota, T. Nishijima, I. Kita, Effects of acute treadmill running at different intensities on activities of serotonin and corticotropin-releasing factor neurons, and anxiety- and depressive-like behaviors in rats. *Behavioural Brain Research* **298**, 44–51 (2016).
34. R. Morikawa, N. Kubota, S. Amemiya, T. Nishijima, I. Kita, Interaction between intensity and duration of acute exercise on neuronal activity associated with depression-related behavior in rats. *Journal of Physiological Sciences* **71**, 1–11 (2021).
35. I. Doležalová, J. Kunst, M. Kojan, J. Chrastina, M. Baláž, M. Brázdil, Anterior thalamic deep brain stimulation in epilepsy and persistent psychiatric side effects following discontinuation. *Epilepsy Behav. Rep.* **12**, 100344 (2019).

36. K. A. Young, L. A. Holcomb, U. Yazdani, P. B. Hicks, D. C. German, Elevated Neuron Number in the Limbic Thalamus in Major Depression. *American Journal of Psychiatry* **161**, 1270–1277 (2004).
37. A.-C. Scharf, J. Gronewold, A. Eilers, O. Todica, C. Moenninghoff, T. R. Doeppner, B. de Haan, C. L. Bassetti, D. M. Hermann, Depression and anxiety in acute ischemic stroke involving the anterior but not paramedian or inferolateral thalamus. *Front. Psychol.* **14** (2023).
38. J. M. Fan, K. Woodworth, K. R. Murphy, L. Hinkley, J. L. Cohen, J. Yoshimura, I. Choi, A. G. Tremblay-McGaw, J. Mergenthaler, C. H. Good, P. A. Pellionisz, A. M. Lee, T. Di Ianni, L. P. Sugrue, A. D. Krystal, Thalamic transcranial ultrasound stimulation in treatment resistant depression. *Brain Stimul.* **17**, 1001–1004 (2024).
39. J. Thundyil, D. Pavlovski, C. G. Sobey, T. V. Arumugam, Adiponectin receptor signalling in the brain. *Br. J. Pharmacol.* **165**, 313–327 (2012).
40. E. Guillod-Maximin, A. F. Roy, C. M. Vacher, A. Aubourg, V. Bailleux, A. Lorsignol, L. Pénicaud, M. Parquet, M. Taouis, Adiponectin receptors are expressed in hypothalamus and colocalized with proopiomelanocortin and neuropeptide Y in rodent arcuate neurons. *Journal of Endocrinology* **200**, 93–105 (2009).
41. A. A. Pratap, R. M. D. Holsinger, Altered Brain Adiponectin Receptor Expression in the 5XFAD Mouse Model of Alzheimer's Disease. *Pharmaceuticals* **13**, 150 (2020).
42. J. Clain, D. Couret, C. Planesse, P. Krejbich-Trotot, O. Meilhac, C. Lefebvre d'Hellencourt, W. Viranaicken, N. Diotel, Distribution of Adiponectin Receptors in the Brain of Adult Mouse: Effect of a Single Dose of the Adiponectin Receptor Agonist, AdipoRON, on Ischemic Stroke. *Brain Sci.* **12**, 680 (2022).
43. C. Li, F. Meng, J. C. Garza, J. Liu, Y. Lei, S. A. Kirov, M. Guo, X. Y. Lu, Modulation of depression-related behaviors by adiponectin AdipoR1 receptors in 5-HT neurons. *Mol. Psychiatry*, doi: 10.1038/s41380-020-0649-0 (2020).
44. F. Sun, Y. Lei, J. You, C. Li, L. Sun, J. Garza, D. Zhang, M. Guo, P. E. Scherer, D. Lodge, X.-Y. Lu, Adiponectin modulates ventral tegmental area dopamine neuron activity and anxiety-related behavior through AdipoR1. *Mol. Psychiatry* **24**, 126–144 (2018).
45. R. R. Kraemer, K. S. Aboudehen, A. K. Carruth, R. T. J. Durand, E. O. Acevedo, E. P. Hebert, L. G. Johnson, V. D. Castracane, Adiponectin responses to continuous and progressively intense intermittent exercise. *Med. Sci. Sports Exerc.* **35**, 1320–5 (2003).
46. Y. Arita, S. Kihara, N. Ouchi, M. Takahashi, K. Maeda, J. Miyagawa, K. Hotta, I. Shimomura, T. Nakamura, K. Miyaoka, H. Kuriyama, M. Nishida, S. Yamashita, K. Okubo, K. Matsubara, M. Muraguchi, Y. Ohmoto, T. Funahashi, Y. Matsuzawa, Paradoxical decrease of an adipose-specific protein, adiponectin, in obesity. *Biochem. Biophys. Res. Commun.* **257**, 79–83 (1999).
47. M. Schön, Z. Kovaničová, Z. Košutzká, M. Nemec, M. Tomková, L. Jacková, D. Máderová, L. Slobodová, P. Valkovič, J. Ukropec, B. Ukropcová, Effects of running on adiponectin, insulin and cytokines in cerebrospinal fluid in healthy young individuals. *Sci. Rep.* **9** (2019).
48. J. Jürimäe, P. Hofmann, T. Jürimäe, J. Mäestu, P. Purge, M. Wonisch, R. Pokan, S. P. von Duvillard, Plasma Adiponectin Response to Sculling Exercise at Individual Anaerobic Threshold in College Level Male Rowers. *Int. J. Sports Med.* **27**, 272–277 (2006).
49. J. Jürimäe, P. Purge, T. Jürimäe, Adiponectin is altered after maximal exercise in highly trained male rowers. *Eur. J. Appl. Physiol.* **93**, 502–5 (2005).
50. F. X. Vollenweider, K. H. Preller, Psychedelic drugs: neurobiology and potential for treatment of psychiatric disorders. *Nat. Rev. Neurosci.* **21**, 611–624 (2020).
51. E. Bromet, L. H. Andrade, I. Hwang, N. A. Sampson, J. Alonso, G. de Girolamo, R. de Graaf, K. Demyttenaere, C. Hu, N. Iwata, A. N. Karam, J. Kaur, S. Kostyuchenko, J. P. Lépine, D. Levinson, H. Matschinger, M. E. M. Mora, M. O. Browne, J. Posada-Villa, M.

C. Viana, D. R. Williams, R. C. Kessler, Cross-national epidemiology of DSM-IV major depressive episode. *BMC Med.* **9** (2011).
52. Z. Iqbal, J. M. Rosa, J. Yu, T. Cheng, D. A. Formolo, A. Hussain, T. P. Wong, T. M. C. Lee, K. So, S.-Y. Yau, Maternal exercise enhances hippocampal plasticity and resilience against stress-induced depressive behaviors in adult offspring. *Sci. Rep.* **16**, 17985 (2026).
53. J. Yu, T. Cheng, H. Guo, Z. Song, Y. Zhong, T. H. Lee, J. Li, D. A. Formolo, A. Hussain, K. Le, Y. Yao, R. L. Abel, W.-H. Cheung, K. Lin, A. Xu, K. K.-Y. Cheng, S.-Y. Yau, How muscle talks to brain: apelin protein mediates exercise-induced antidepressant effects. *Mol. Psychiatry*, doi: 10.1038/s41380-026-03651-y (2026).
54. T. H. Lee, M. Devaki, D. A. Formolo, J. M. Rosa, A. S. K. Cheng, S. Y. Yau, Effects of Voluntary Wheel Running Exercise on Chemotherapy-Impaired Cognitive and Motor Performance in Mice. *Int. J. Environ. Res. Public Health* **20** (2023).
55. S. Y. Yau, T. H. Y. Lee, D. A. Formolo, W. L. Lee, L. C. K. Li, P. M. Siu, C. C. H. Chan, Effects of maternal voluntary wheel running during pregnancy on adult hippocampal neurogenesis,temporal order memory, and depression-like behavior in adult female and male offspring. *Front. Neurosci.* **13** (2019).
56. S. D. Suarez, G. G. Gallup, An ethological analysis of open-field behavior in rats and mice. *Learn. Motiv.* **12**, 342–363 (1981).
57. T. D. Gould, *Mood and Anxiety Related Phenotypes in Mice* (Humana Press, Totowa, NJ, 2009; http://link.springer.com/10.1007/978-1-60761-303-9)vol. 42 of *Neuromethods*.
58. B. L. Roth, DREADDs for Neuroscientists. *Neuron* **89**, 683–694 (2016).
59. B. Zingg, X. Chou, Z. Zhang, L. Mesik, F. Liang, H. W. Tao, L. I. Zhang, AAV-Mediated Anterograde Transsynaptic Tagging: Mapping Corticocollicular Input-Defined Neural Pathways for Defense Behaviors. *Neuron* **93**, 33–47 (2017).
60. E. S. Boyden, F. Zhang, E. Bamberg, G. Nagel, K. Deisseroth, Millisecond-timescale, genetically targeted optical control of neural activity. *Nat. Neurosci.* **8**, 1263–1268 (2005).
61. O. Yizhar, L. E. Fenno, T. J. Davidson, M. Mogri, K. Deisseroth, Optogenetics in Neural Systems. [Preprint] (2011). https://doi.org/10.1016/j.neuron.2011.06.004.
62. George. Paxinos, K. B. Franklin, *The Mouse Brain in Stereotaxic Coordinates* (Academic Press, San Diego, ed. 2nd, 2001).
63. D. A. Formolo, T. H. Lee, J. Yu, K. Lin, G. Chen, G. S. Kranz, S.-Y. Yau, Increasing Adiponectin Signaling by Sub-Chronic AdipoRon Treatment Elicits Antidepressant- and Anxiolytic-Like Effects Independent of Changes in Hippocampal Plasticity. *Biomedicines* **11**, 249 (2023).
64. K. J. Friston, S. Williams, R. Howard, R. S. J. Frackowiak, R. Turner, Movement-Related effects in fMRI time-series. *Magn. Reson. Med.* **35**, 346–355 (1996).
65. N. Tzourio-Mazoyer, B. Landeau, D. Papathanassiou, F. Crivello, O. Etard, N. Delcroix, B. Mazoyer, M. Joliot, Automated Anatomical Labeling of Activations in SPM Using a Macroscopic Anatomical Parcellation of the MNI MRI Single-Subject Brain. *Neuroimage* **15**, 273–289 (2002).

Acknowledgments

We thank the research support from the core facilities, including University Behavioural and System Neuroscience (UBSN), University Research Facility in Life Sciences (ULS), Central Animal Facilities of the Hong Kong Polytechnic University (CAF) and PolyU Shenzhen Research Institute (SZRI).

Funding

This work is supported by Strategic Topics Grant (UGC; STG1/M-501/23-N), General Research Fund (GRF 15100018) from the University Grants Committee, National Science Foundation of China (NSFC 81801346) and project seed fund from Mental Health Research Center (MHRC) and Research Institute of Smart Ageing (RISA).

Author contributions

Conceptualization: SYY

Methodology: DAF, TC, ZI, JY, NF, HZ, GSK

Investigation: DAF, TC, JY, ZI, NF

Visualization: DAF, TC, HZ, GSK

Supervision: SYY

Writing—original draft: DAF, TC

Writing—review & editing: DAF, TC, SYY

Competing Interest

The authors declare they have no competing interests.

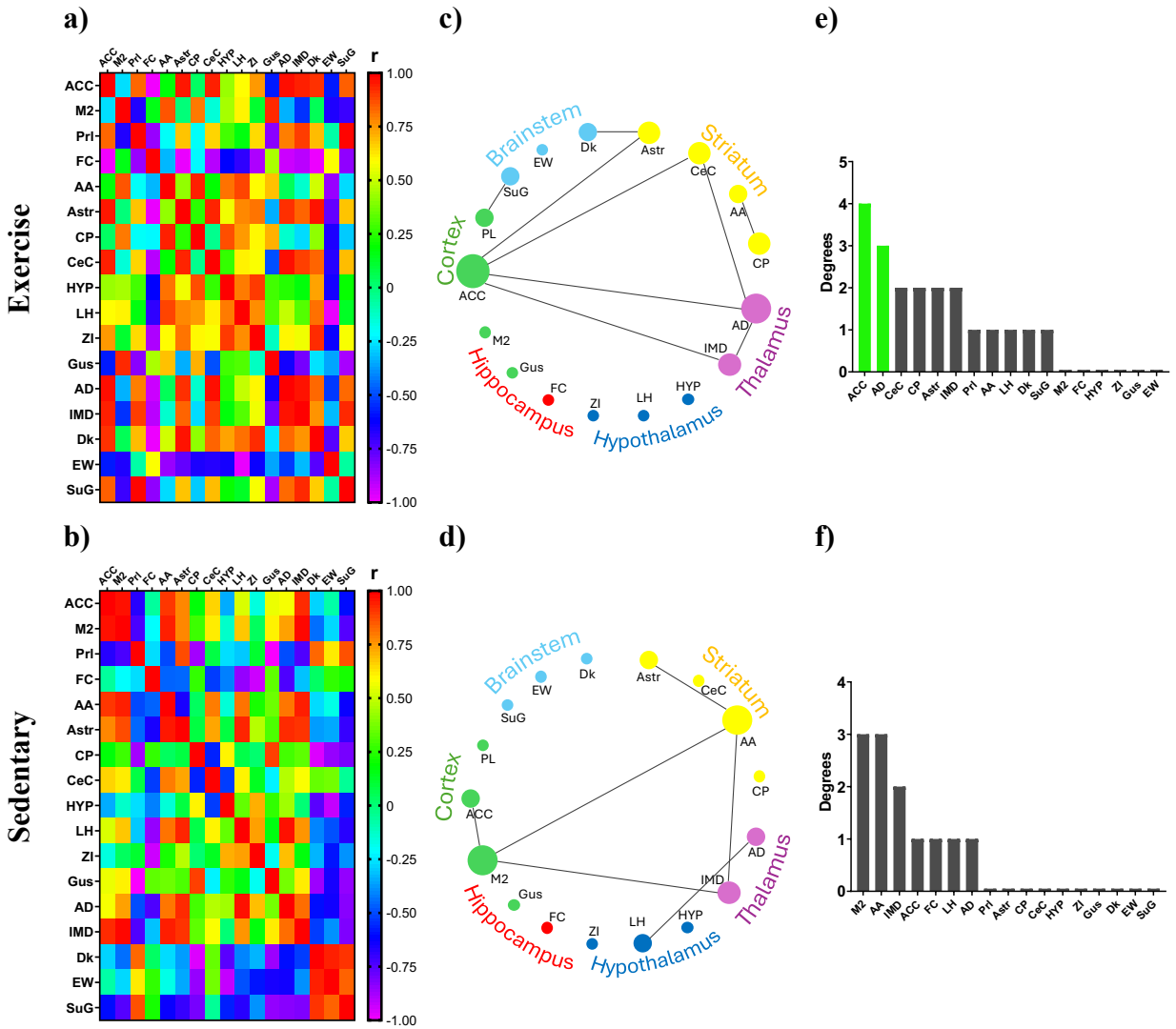


Fig. 1. The ACC and AD are high-degree nodes involved in the exercise-associated functional network. Functional correlation matrix of c-Fos expression levels in (**a**) exercised and (**b**) sedentary mice across the seventeen brain regions significantly modulated by physical exercise. Suprathreshold correlations ($r > 0.83$, $p < 0.05$) were included in the brain graphs as edges connecting the nodes (brain regions) for (**c**) exercise and (**d**) sedentary mice. Degree centrality is presented as the probability distribution of the number of edges incurring on nodes for (**e**) exercise and (**f**) sedentary mice. The 75th percentile (degree > 2) was used as a cutoff point to select high-degree nodes. C-Fos expression raw data were extracted from (9).

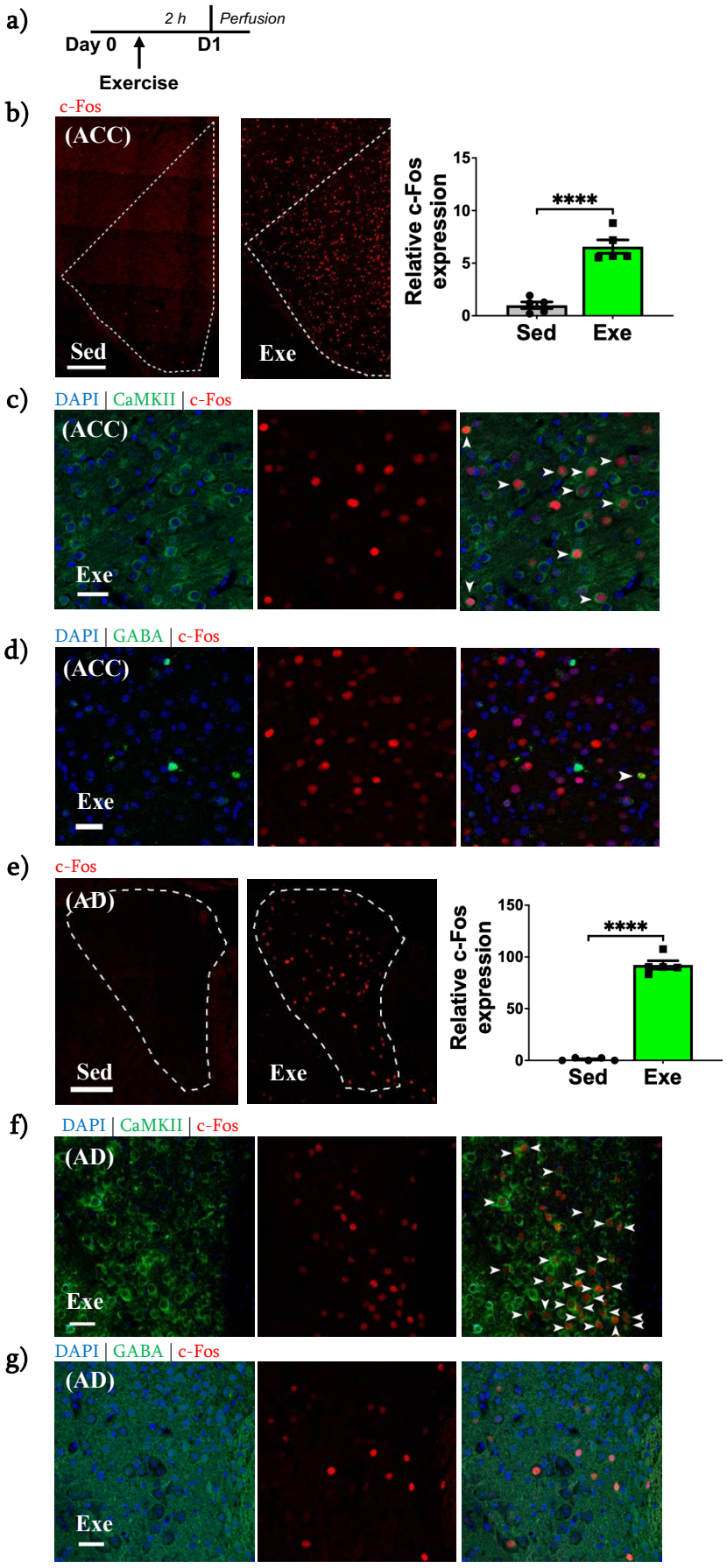

a)
2 h
Perfusion
Day 0
D1
Exercise
b)
c-Fos
(ACC)
Sed
Exe
Relative c-Fos expression
15
10
5
0
****
Sed
Exe
c)
DAPI | CaMKII | c-Fos
(ACC)
Exe
d)
DAPI | GABA | c-Fos
(ACC)
Exe
e)
c-Fos
(AD)
Sed
Exe
Relative c-Fos expression
150
100
50
0
****
Sed
Exe
f)
DAPI | CaMKII | c-Fos
(AD)
Exe
g)
DAPI | GABA | c-Fos
(AD)
Exe

Fig. 2. A single bout of physical exercise activates glutamatergic neurons in the ACC and AD. (**a**) Experimental timeline. Animals were sacrificed two hours after a single bout of running exercise for immunohistochemical analyses. (**b**) Relative expression of c-Fos in the ACC of exercised compared to sedentary mice (n = 5/group, scale bar: 200 μm). Co-expression of c-Fos with (**c**) CaMKII as a glutamatergic marker and (**d**) GABA as a GABAergic marker in the ACC of exercised mice (scale bars: 30 μm). (**e**) Relative expression of c-Fos in the AD of exercised compared to sedentary mice (n = 5/group, scale bar: 100 μm). Co-expression of c-Fos with (**f**) CaMKII and (**g**) GABA in the AD of exercised mice (scale bars: 30 μm). Data presented as mean ± SEM; unpaired t-test, **** $p < 0.0001$.

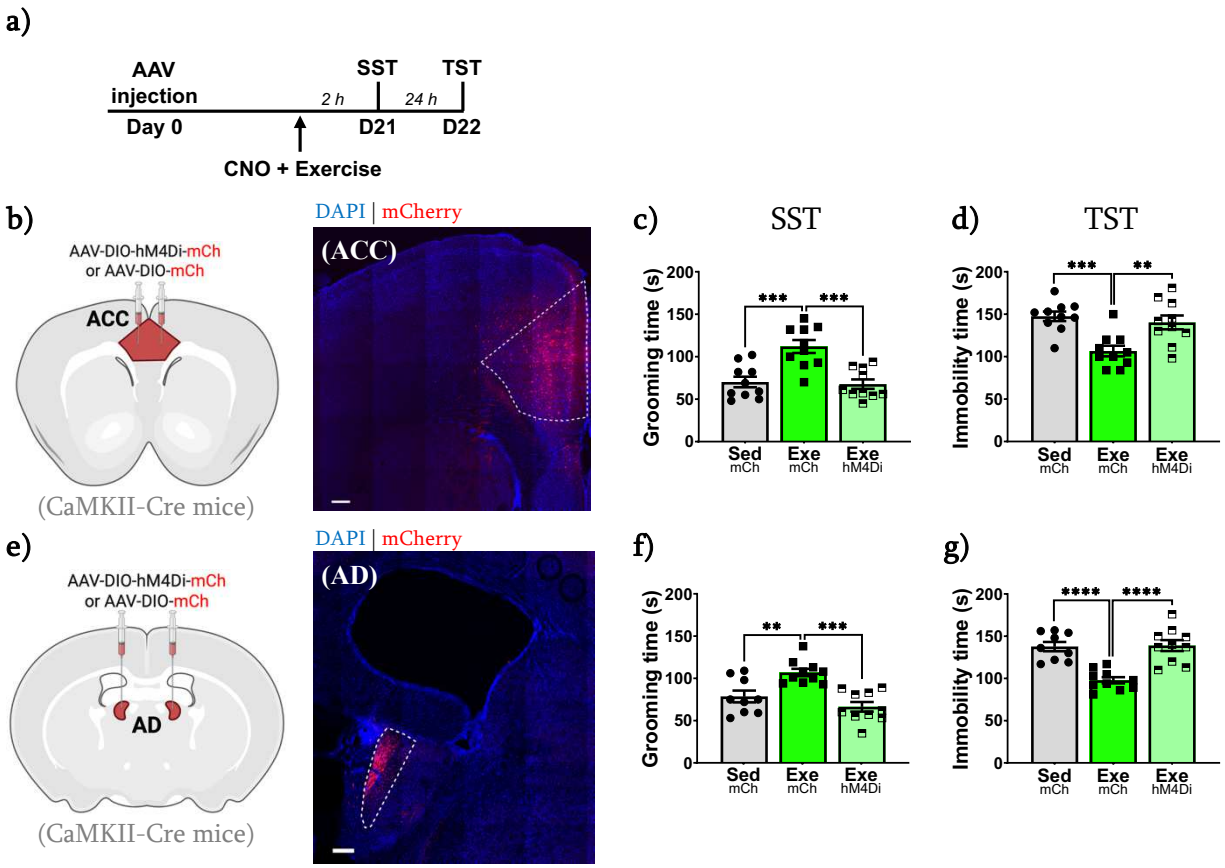


Fig. 3. Activation of glutamatergic neurons in the ACC or AD is required for the rapid antidepressant-like effects of single-bout physical exercise. (**a**) Experimental timeline. CaMKII-Cre mice were injected with AAV-DIO-hM4Di-mCh or AAV-DIO-mCh as a control. Animals were treated with CNO (1 mg/kg, i.p.) 30 minutes before the exercise protocol, followed by behavioral assessments 2 and 24 hours later. (**b**) Injection site (left) and representative image (right) of virus expression in the ACC (scale bar: 200 μm). (**c**) Expression of grooming time in the SST (2-hour timepoint) and (**d**) immobility time in the TST (24-hour timepoint) after exercise (n = 10/group). (**e**) Injection site (left) and representative image (right) of virus expression in the AD (scale bar: 200 μm). (**f**) Expression of grooming time in the SST and (**g**) immobility time in the TST after exercise (n = 9-10/group). Data presented as mean ± SEM; One-way ANOVA followed by Tukey's test for multiple comparisons, **, $p < 0.01$, *** $p < 0.001$, **** $p < 0.0001$.

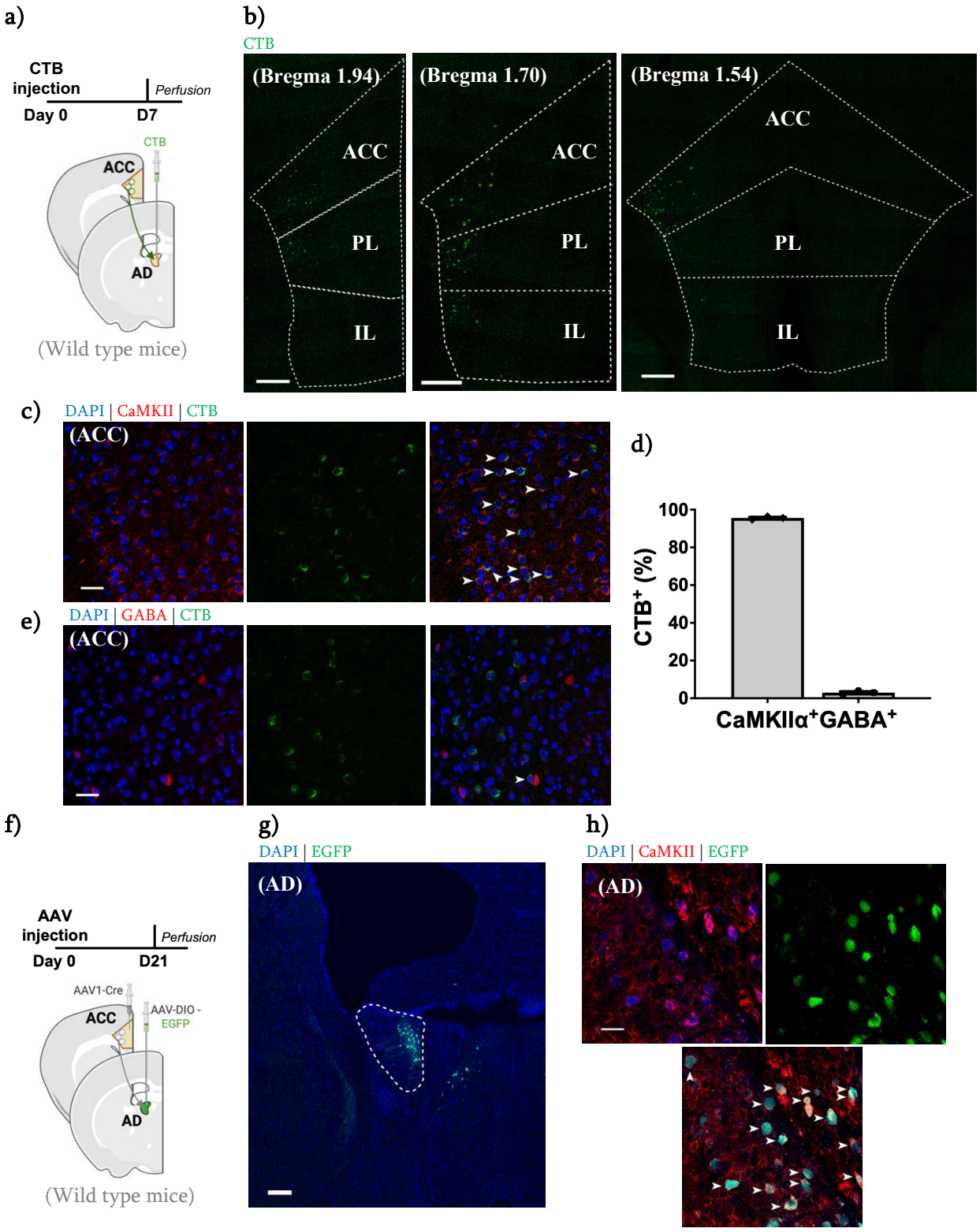
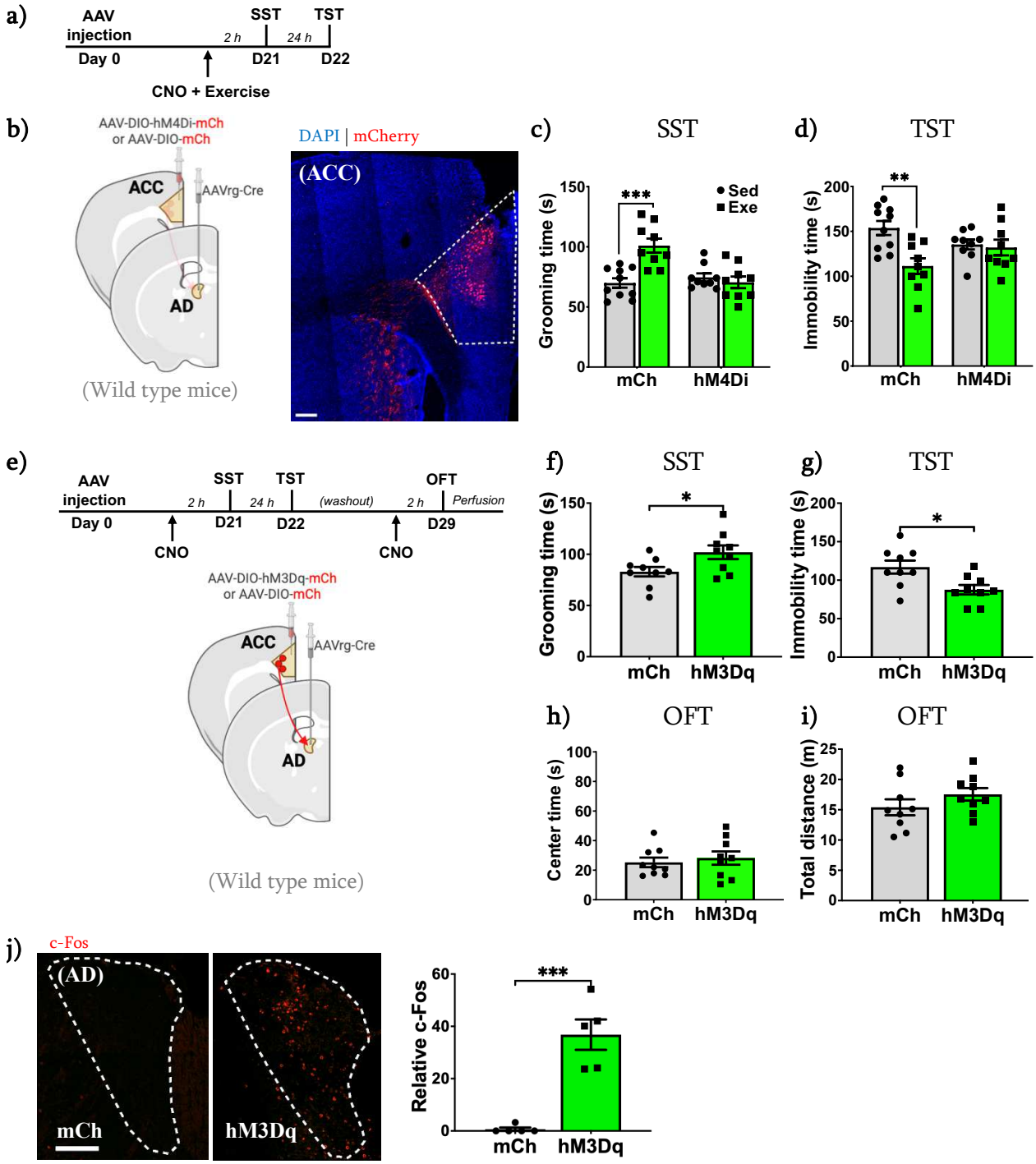


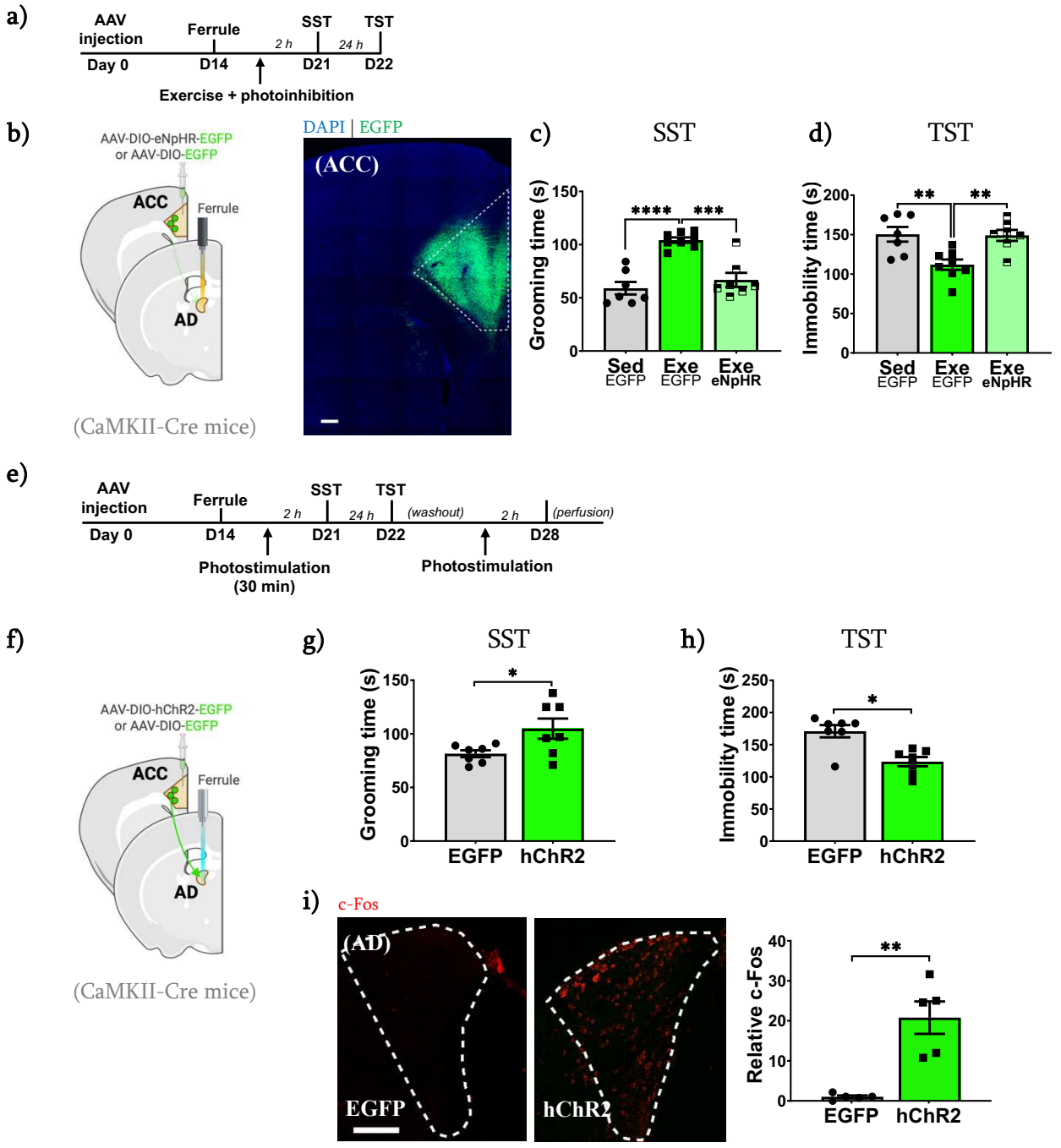
Fig. 4. The ACC sends glutamatergic projections to the AD. (**a**) Experimental timeline and CTB injection site. CTB was unilaterally injected into the AD while animals were sacrificed 7 days later for immunohistochemical analysis. (**b**) Representative images of CTB expression along the ACC anteroposterior axis (scale bars: 200 μm). Co-expression of CTB with (**c**) CaMKII and (**d**) GABA in the ACC (scale bars: 30 μm). (**e**) Proportion of CTB^+ cells co-

expressing CaMKII or GABA in the ACC (n = 3); data presented as mean ± SEM. (**f**) Experimental timeline. The anterograde AAV1 was unilaterally injected in the ACC, while a Cre-dependent AAV driving the expression of EGFP was injected ipsilaterally in the AD. Animals were sacrificed 21 days later for immunohistochemical analysis. (**g**) Representative image of virus expression in the AD (scale bar: 200 μm). (**h**) Co-expression of EGFP with CaMKII in the AD (scale bars: 30 μm).



1056 **Fig. 5. The ACC-AD pathway mediates the rapid antidepressant-like effects of single-bout**
1057 **physical exercise.** (**a**) Experimental timeline for circuit inhibition. Mice were injected with
1058 AAVrg-Cre in the AD, and AAV-DIO-hM4Di-mCh or AAV-DIO-mCh in the ACC. Animals
1059 were treated with CNO (1 mg/kg, i.p.) 30 minutes before the exercise protocol, followed by
1060 behavioral assessment. (**b**) Injection site (left) and representative image of virus expression in the
1061 ACC (right) (scale bar: 200 μm). (**c**) Expression of grooming time in the SST and (**d**) immobility
1062 time in the TST after exercise (n = 9-10/group). (**e**) Experimental timeline for circuit activation

(top) and injection site using AAV-DIO-hM3Dq-mCh (bottom). (**f**) Expression of grooming time in the SST and (**g**) immobility time in the TST after CNO treatment (n = 9/group). (**h**) Time spent in the center and (**i**) total distance traveled in the OFC 2 h after CNO treatment (n = 9/group). (**j**) Relative c-Fos expression in the AD after CNO treatment (n = 5/group, scale bar: 100 μm). Data presented as mean ± SEM; data analyzed by two-way ANOVA followed by Tukey's test for multiple comparisons (4 groups) or unpaired t-test (2 groups), * $p < 0.05$, ** $p < 0.01$, *** $p < 0.001$.



1072 **Fig. 6. Optogenetic modulation of the ACC-AD circuit in exercised and sedentary mice.** (**a**)
1073 Experimental timeline for optogenetic inhibition of the ACC-AD circuit. CaMKII-Cre mice were
1074 injected with AAV-DIO-eNpHR-EGFP or AAV-DIO-EGFP in the ACC, while ferrules were
1075 implanted above the AD. Photoinhibition was performed only during the exercise protocol,
1076 followed by behavioral assessment. (**b**) Injection and ferrule implantation sites (left) and
1077 representative image of virus expression in the ACC (right) (scale bar: 200 μm). (**c**) Expression
1078 of grooming time in the SST and (**d**) immobility time in the TST after exercise (n = 7-8/group).
1079 (**e**) Experimental timeline for optogenetic activation of the ACC-AD circuit and (**e**) injection site
1080 using AAV-DIO-hChR2-mCh. Photostimulation was performed for 30 minutes, followed by

behavioral assessment, and repeated a second time before euthanasia. (**g**) Expression of grooming time in the SST and (**h**) immobility time in the TST after exercise (n = 7/group). (**i**) Relative c-Fos expression in the AD after photostimulation (n = 5/group, scale bar: 100 μm). Data presented as mean ± SEM; data analyzed by one-way ANOVA followed by Tukey's test for multiple comparisons (3 groups) or unpaired t-test (2 groups), * $p < 0.05$, ** $p < 0.01$, *** $p < 0.001$, **** $p < 0.0001$.

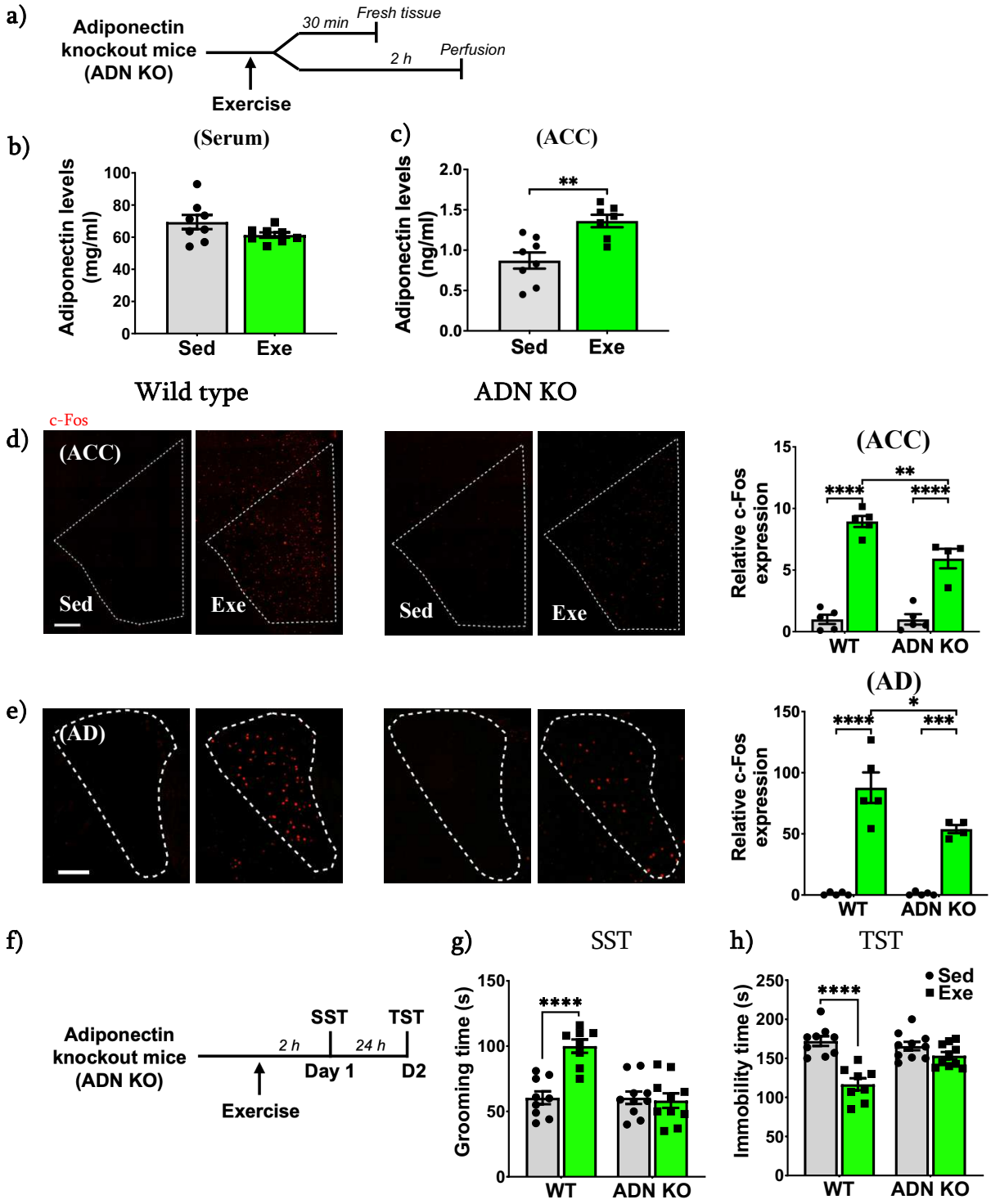


Fig. 7. Adiponectin deficiency impairs the exercise-induced rapid activation of the ACC and AD regions. (**a**) Experimental timeline. Adiponectin knockout (ADN KO) and wild-type (WT) mice underwent the exercise protocol, followed by the collection of fresh and perfused tissue at different time points. (**b**) Adiponectin levels in the serum and (**c**) ACC after exercise. (**d**) Relative c-Fos expression in the ACC and (**e**) AD (n = 5/group, scale bars: 200 μm [ACC] and 100 μm [AD]). (**f**) In another cohort of ADN KO and WT mice, animals underwent the exercise protocol, followed by behavioral assessment. (**g**) Expression of grooming time in the

SST and (**h**) immobility time in the TST after exercise (n = 8-10/group). Data presented as mean ± SEM; data analyzed by two-way ANOVA followed by Tukey's test for multiple comparisons (4 groups) or unpaired t-test (2 groups), * $p < 0.05$, ** $p < 0.01$, *** $p < 0.001$, **** $p < 0.0001$.

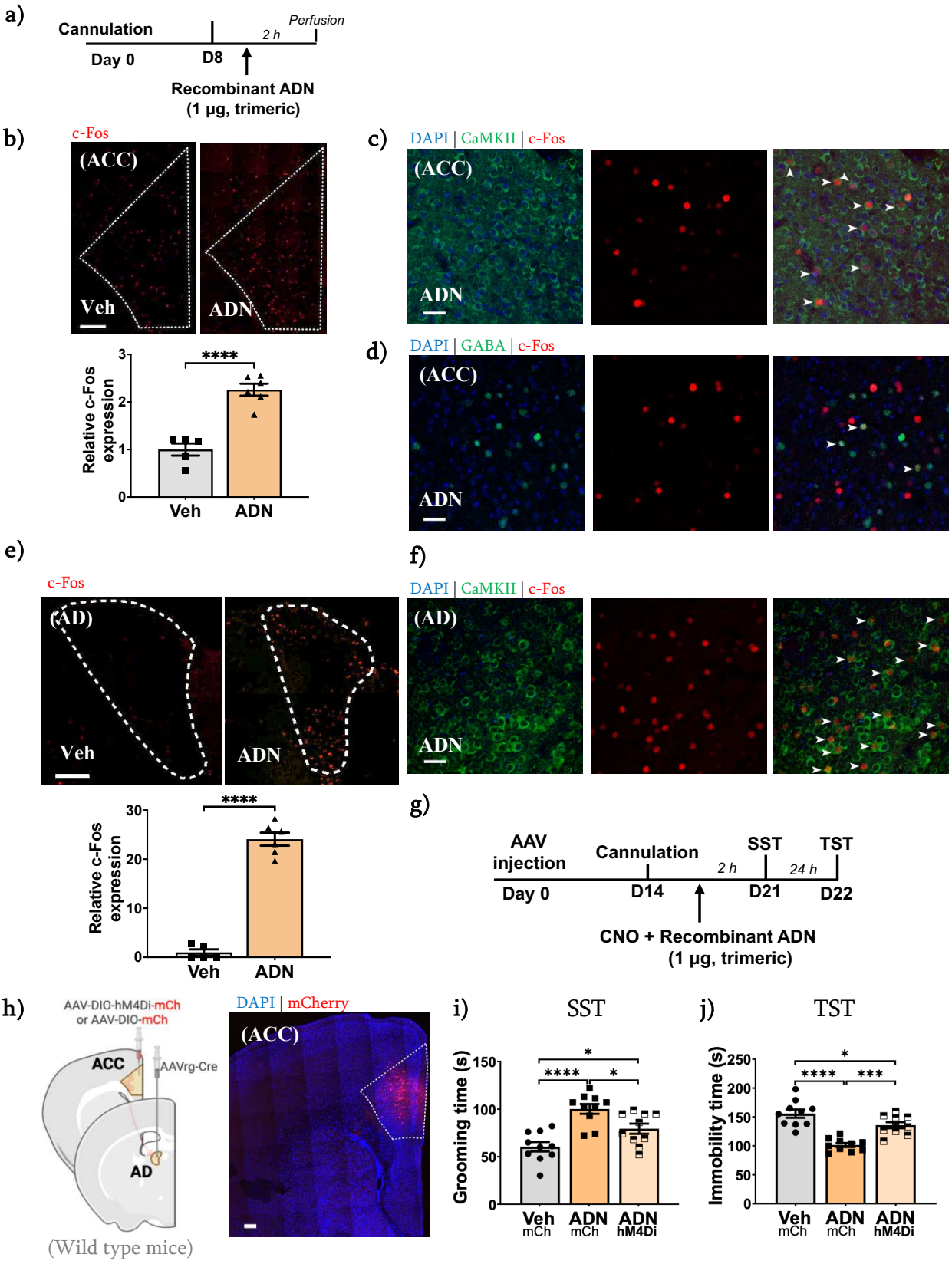


Fig. 8. The ACC-AD pathway is involved in the rapid antidepressant effects induced by intracerebroventricular infusion of recombinant adiponectin. (**a**) Experimental timeline. Cannulated mice received a single intracerebroventricular infusion of recombinant adiponectin (1

μg, trimeric) or vehicle 2 hours before perfusion. (**b**) Relative c-Fos expression in the ACC (n = 5-6/group, scale bar: 200 μm). (**c**) Co-expression of c-Fos with CaMKII and (**d**) GABA in the ACC (scale bars: 30 μm). (**e**) Relative c-Fos expression in the AD (n = 5-6/group, scale bar: 100 μm). (**f**) Co-expression of c-Fos with CaMKII in the AD (scale bar: 30 μm). (**g**) Another cohort of mice was injected with AAVrg-Cre in the AD and with AAV-DIO-hM4Di-mCh or AAV-DIO-mCh in the ACC, with cannulation occurring 14 days after virus injection. Seven days after cannulation, animals were treated with CNO (1 mg/kg, i.p.) 30 minutes before intracerebroventricular infusion of recombinant adiponectin (1 μg, trimeric), followed by behavioral assessment. (**h**) Injection site (left) and representative image of viral expression in the ACC (right, scale bar: 200 μm). (**i**) Expression of grooming time in the SST and (**j**) immobility time in the TST (n = 10/group). Data presented as mean ± SEM; unpaired t-test (B and E), one-way ANOVA followed by Tukey's test for multiple comparisons (I and J), * $p < 0.05$, ** $p < 0.01$, **** $p < 0.0001$.

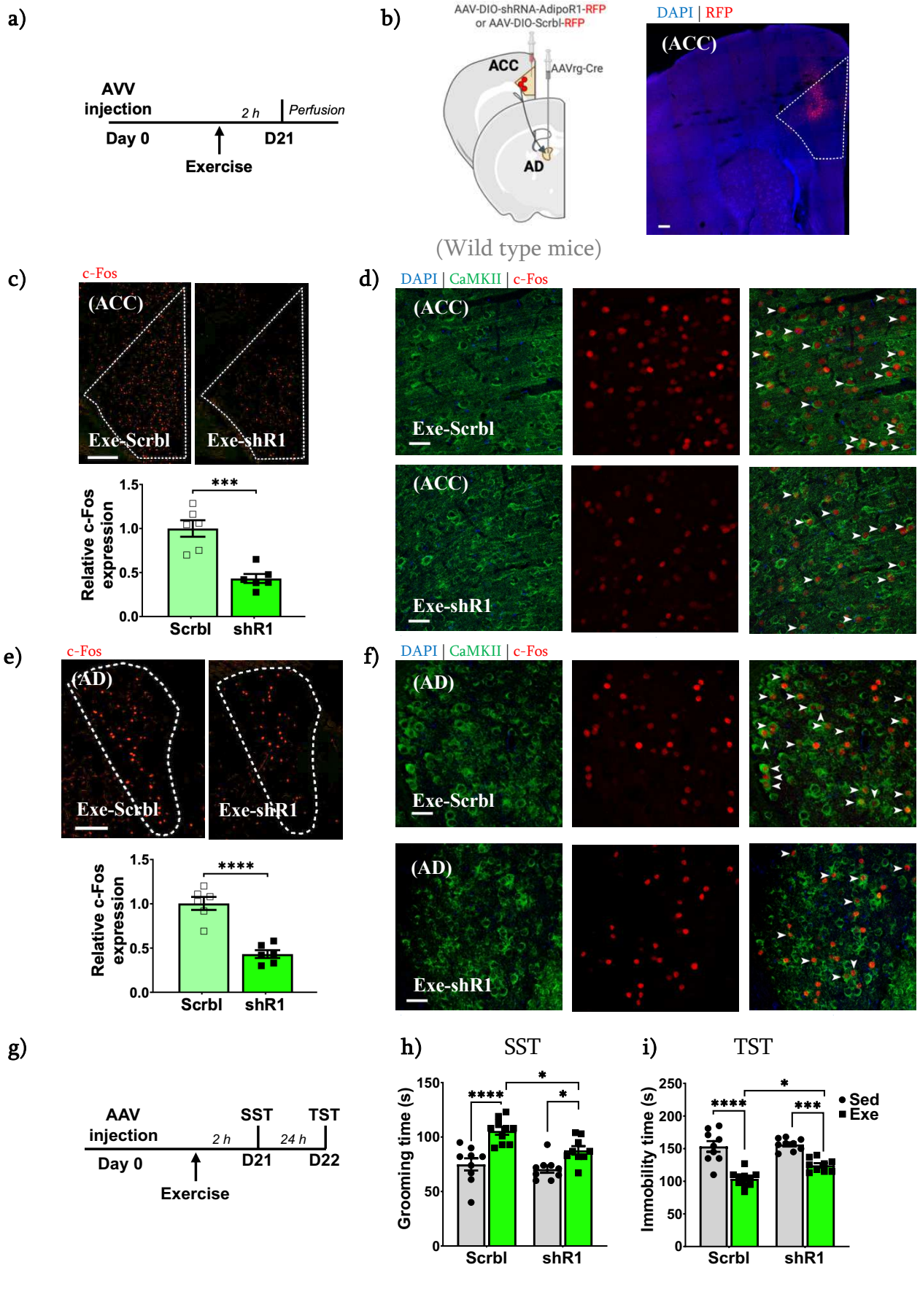
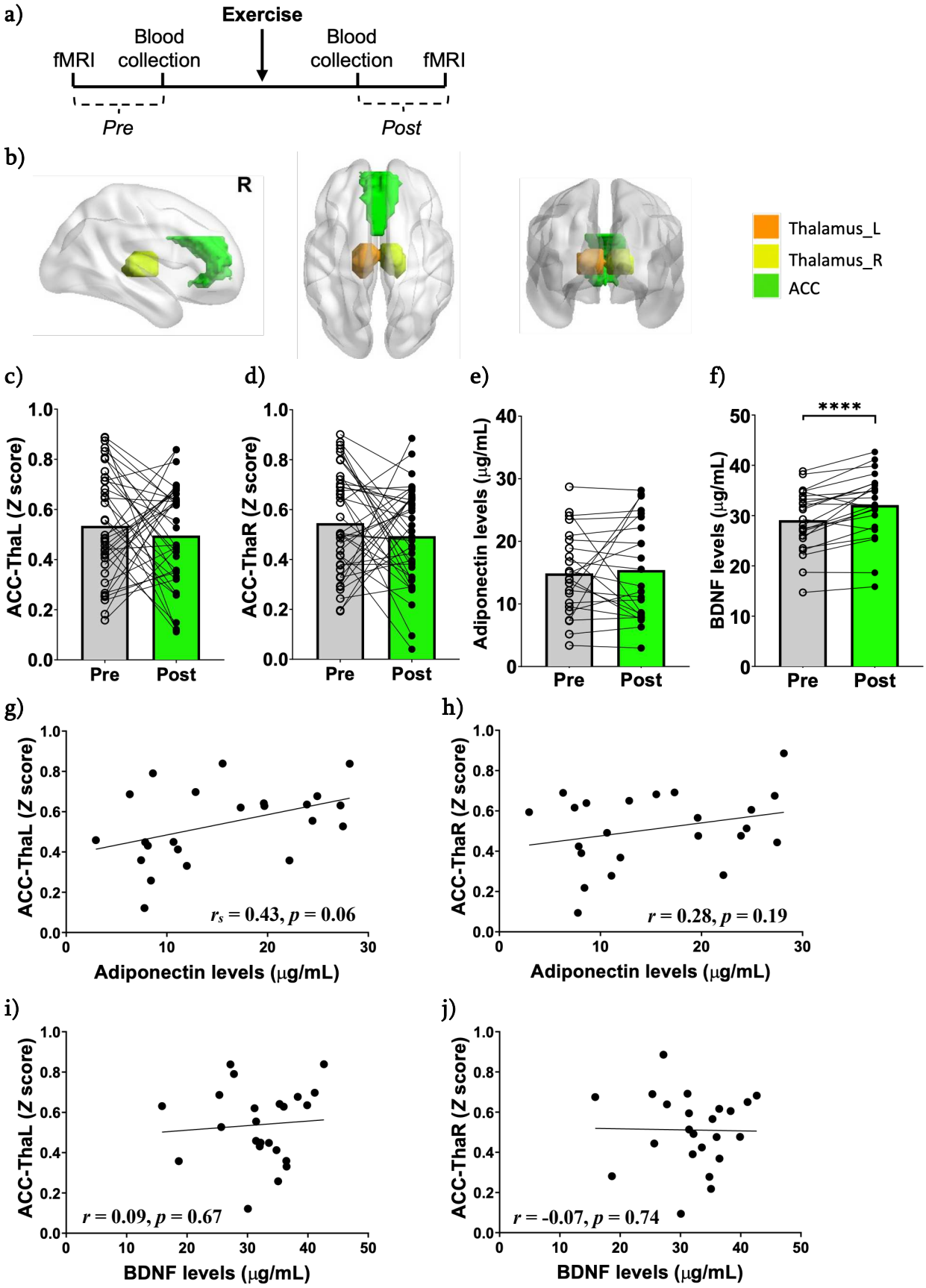

a)
AVV injection
2 h
Perfusion
Day 0
D21
Exercise
b)
AAV-DIO-shRNA-AdipoR1-RFP or AAV-DIO-Scrbl-RFP
ACC
AAVrg-Cre
AD
DAPI | RFP
(ACC)
(Wild type mice)
c)
c-Fos
(ACC)
Exe-Scrbl
Exe-shR1
Relative c-Fos expression
***
Scrbl
shR1
d)
DAPI | CaMKII | c-Fos
(ACC)
Exe-Scrbl
(ACC)
Exe-shR1
e)
c-Fos
(AD)
Exe-Scrbl
Exe-shR1
Relative c-Fos expression
****
Scrbl
shR1
f)
DAPI | CaMKII | c-Fos
(AD)
Exe-Scrbl
(AD)
Exe-shR1
g)
AAV injection
SST
TST
2 h
24 h
Day 0
D21
D22
Exercise
h)
SST
Grooming time (s)
****
*
*
Scrbl
shR1
i)
TST
Immobility time (s)
****
*
***
Sed
Exe
Scrbl
shR1

Fig. 9. Acute exercise activates the ACC-AD circuit via adiponectin-AdipoR1 signaling. (**a**) Experimental timeline. AAVrg-Cre was injected into the AD of wild-type mice, and AAV-DIO-shRNA-AdipoR1-RFP or AAV-DIO-shRNA-Scrbl-RFP was injected into the ACC to knock down AdipoR1 in the ACC-AD projections. Three weeks later, animals were subjected to the exercise protocol two hours before perfusion. (**b**) Injection site and representative image of virus expression in the ACC (scale bar: 200 μm). (**c**) Relative c-Fos expression in the ACC (n = 6/group, scale bar: 200 μm). (**d**) Co-expression of c-Fos with CaMKII in control (Scrbl) and knockdown (shR1) exercised mice in the ACC (scale bars: 30 μm). (**e**) Relative c-Fos expression in the AD (n = 6/group, scale bar: 100 μm). (**f**) Co-expression of c-Fos with CaMKII in control (Scrbl) and knockdown (shR1) exercised mice in the AD (scale bars: 30 μm). (**g**) In a separate cohort of mice, knockdown of AdipoR1 was performed in the ACC-AD projections, and animals were subjected to behavioral assessment after the exercise protocol. (**h**) Expression of grooming time in the SST and (**i**) immobility time in the TST after exercise (n = 9-10/group). Data presented as mean ± SEM; data analyzed by unpaired t-test (2 groups) or two-way ANOVA followed by Tukey's test for multiple comparisons (4 groups). * $p < 0.05$, *** $p < 0.001$, **** $p < 0.0001$.



1136 **Fig. 10. Post-exercise adiponectin levels are correlated with frontothalamic functional**
1137 **connectivity in young adults.** (**a**) Single-arm, pre-posttest study design. Participants (n = 40)

underwent functional magnetic resonance imaging (fMRI), followed by blood collection before (pre-test) and after (post-test) a single 30-min moderate-intensity treadmill running exercise session. (**b**) Pre-post comparison of functional connectivity between the anterior cingulate cortex (ACC) and the left and (**c**) right thalamus (n = 39). (**d**) Pre-post comparison of adiponectin and (**e**) BDNF levels (n = 23). (**f**) Linear correlation between post-exercise adiponectin levels and the ACC-left thalamus and (**g**) ACC-right thalamus functional connectivity (n = 23). (**h**) Linear correlation between post-exercise BDNF levels and the ACC-left thalamus and (**i**) ACC-right thalamus functional connectivity (n = 23). Data presented as mean ± SEM; data analyzed by unpaired t-test (D and F), Wilcoxon signed-rank test (C and E), Spearman's Rho (g) or Pearson's correlation (h-j). **** $p < 0.0001$.

Supplementary Files

This is a list of supplementary files associated with this preprint. Click to download.

- Supplementarymaterials18.09.26.pdf